Offshore controls on nearshore rip currents

Joseph W. Long and H. Tuba Özkan-Haller

College of Oceanic and Atmospheric Sciences, Oregon State University, Corvallis, Oregon, USA

[1] The rip current field resulting from the transformation of surface gravity waves over offshore submarine canyons is studied. Employing a wave transformation model and a wave-induced circulation model over observed bathymetry we find that wave height variations associated with undulations in the canyon contours cause rip current circulation cells with alongshore spacing of O(100m) even though the nearshore bathymetry displays no variations at these length scales. Further, the predicted rips correspond to observed rip currents during the Nearshore Canyon Experiment (NCEX). Motivated by these results we study the relationship between O(100 m) scale variations in offshore bathymetric contours and the resulting rip current field in the nearshore. To isolate the roles of possible bathymetric features, we construct a series of idealized case studies that include site characteristics found at NCEX that are conducive of rip current development, such as a curved shoreline, an offshore submarine canyon and undulations in the canyon contours. Our results show that the first two components are unable to produce the observed short-scale circulation systems, while wave refraction over undulations in the canyon walls at length scales of O(100 m) provides a sufficient disturbance to generate alongshore wave height variations that drive multiple rip currents for a variety of incident wave conditions. Rips are not generated when the wave period is short, or when the angle of incidence is large. Analysis of the alongshore momentum balances further demonstrates that the rip current locations are also strongly influenced by inertial effects. Hence, nonlinear processes are important within the rip current circulation cell and we find that nonlinear advective acceleration terms balance a large portion of the driving alongshore gradient in the mean water surface elevation in the vicinity of the rip currents with bottom friction accounting for the remainder. Away from the rips, the balance is between the wave forcing and the pressure gradient outside the surf zone and wave forcing and bottom friction inside the surf zone, as expected.

1. Introduction

[2] Rip currents are common features along beaches and are thought to arise from alongshore gradients in wave height and the associated variations in the mean water surface elevation. It is generally understood that the gradients in the water surface elevation that drive the flow could arise from several individual mechanisms that may also work in combination. *Shepard et al.* [1941] made some of the first scientific observations of circulation patterns associated with rip currents off the coast of La Jolla, California, by recording distinct visual signals such as sediment plumes or advected surface foam patterns associated with these intense localized currents. Their studies indicated that wave refraction over the offshore submarine canyons at this site created strong alongshore wave height gradients suitable for rip current generation [*Shepard and Inman*, 1950].

[3] Subsequent studies proposed that other mechanisms can also be responsible for such alongshore wave height gradients. For example, *Bowen* [1969] and *Bowen and Inman* [1969] examined, theoretically and experimentally, how alongshore wave height variations could be caused by standing edge waves. *Dalrymple* [1975] proposed that intersecting wave trains of identical frequency could provide the necessary variations in mean water level required to generate rip currents. In contrast to *Shepard and Inman* [1950], who pointed to variable offshore bathymetry, a laboratory experiment by *Haller et al.* [2002] focused on rip currents generated by alongshore wave height variations caused by nearshore bathymetric variations (in the form of alongshore-uniform nearshore bars that were interrupted by rip channels). Finally, *Hino* [1974] was the first to argue that alongshore variable bathymetry and hydrodynamics could evolve as a result of an instability of the coupled hydrodynamic-morphodynamic system. This is by no means an exhaustive list of the research conducted to study rip current development, but indicates the wide range of mechanisms that have received attention. The focus of this study is to
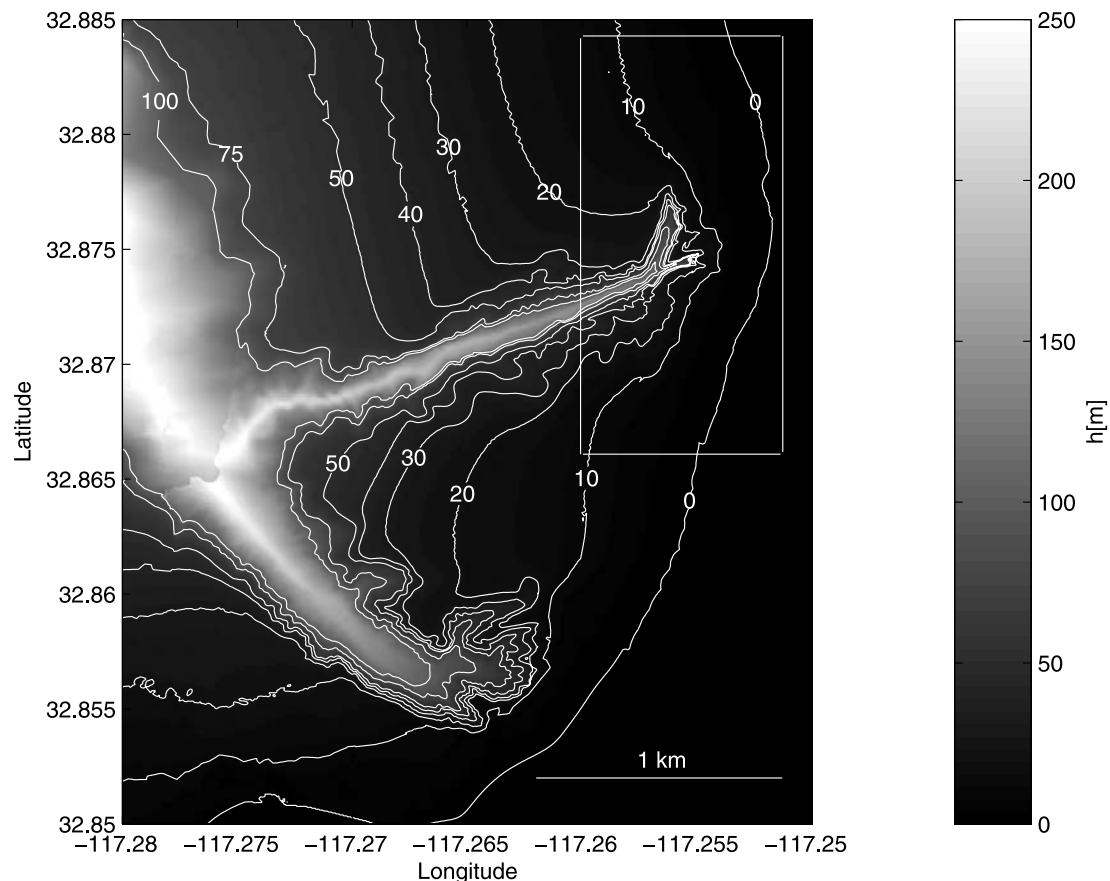
Figure 1. Bathymetry of the site of the Nearshore Canyon Experiment (NCEX) that took place in La Jolla, California, during the fall of 2003.

return to the original site and hypothesis examined by *Shepard and Inman* [1950] regarding wave refraction over offshore features as a mechanism for the development of rip currents. The site studied by *Shepard and Inman* [1950] has recently been the focus of the Nearshore Canyon Experiment (NCEX). Numerical model simulations of the wave field at this site show alongshore variations in wave height over broad regions that can have length scales of up to O(km), consistent with the results of *Shepard and Inman* [1950]. However, the simulations also show smaller scale (O(100 m)) variations, apparently due to variations in the canyon contours at comparable length scales. Further, simulations of the nearshore circulation for these wave conditions show rip currents at locations that are correlated with these smaller-scale variations in wave height and also correspond to rip currents observed during the experiment. Motivated by these results, we will examine and test the hypothesis that variations in the offshore bathymetry at length scales of O(100m) can exert a strong control on the locations of the rip currents at this site. In the following, we first briefly describe the Nearshore Canyon Experiment (section 2) since the observations at this site serve as a motivation to this study. We then utilize numerical models simulating waves and nearshore circulation at this site, point out the correspondence of the rip currents and small-scale variations in the wave height, and show qualitative comparisons to remote sensing observations (section 3). In section 4, we test our hypothesis by decomposing the offshore

bathymetry into the superposition of three idealized components, a curved shoreline, an oblique submarine canyon, and small-scale variations (i.e. undulations) in the offshore bathymetry. An evaluation of alongshore momentum balances inside and outside of the surf zone provides further indication of the forcing mechanisms that lead to the generation of rip currents in each case. These results are followed by a discussion regarding the sensitivity of the nearshore circulation to changes in offshore spectral parameters. A brief discussion and a summary of the conclusions from this study are provided in sections 5 and 6, respectively.

2. Overview of the Nearshore Canyon Experiment

[4] The Nearshore Canyon Experiment (NCEX) was a large-scale field study designed to collect information about surf zone processes in a region where wave transformation was influenced by submarine canyons. Many academic institutions and governmental research agencies contributed to the data collection, which took place between September and December of 2003, with each institution defining its individual deployment period.

2.1. Site Description

[5] The site of the experiment was located along a section of coastline in La Jolla, California, stretching from Point La
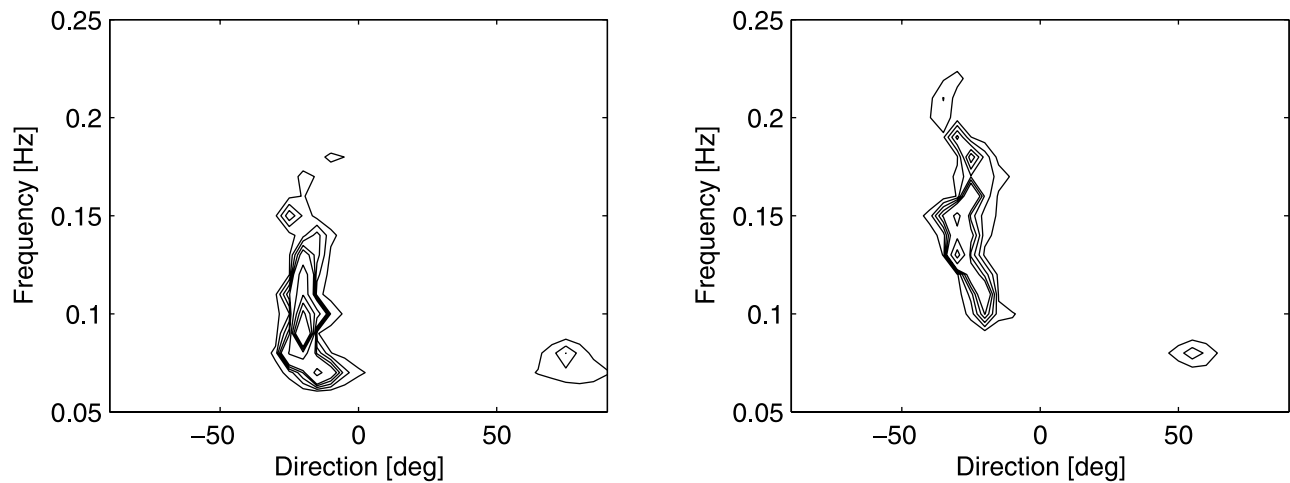
Figure 2. Variance density (m2/Hz/degree) of the wave spectra collected at the offshore wave buoy for October 10, 2003 at 1900 GMT (left) and October 31, 2003 at 1500 GMT (right). Contour lines of variance density correspond to the 0, 0.01, 0.02, 0.03, 0.04, 0.05, 0.1, 0.15, 0.2, and 0.25 m2/Hz/degree contours.

Jolla northward to Torrey Pines Beach (Figure 1). The site is characterized by the presence of a submarine canyon that divides into two branches near the coast with the Scripps Canyon situated to the north and the La Jolla Canyon to the south. The Scripps Canyon has an unusual feature at the

canyon tip often referred to as the canyon boot and the walls of both canyons have undulations that are especially evident in the 30 and 40 m contours. Blacks Beach, denoted by the rectangular border in Figure 1, is located directly east extending northward from Scripps Canyon and is a region
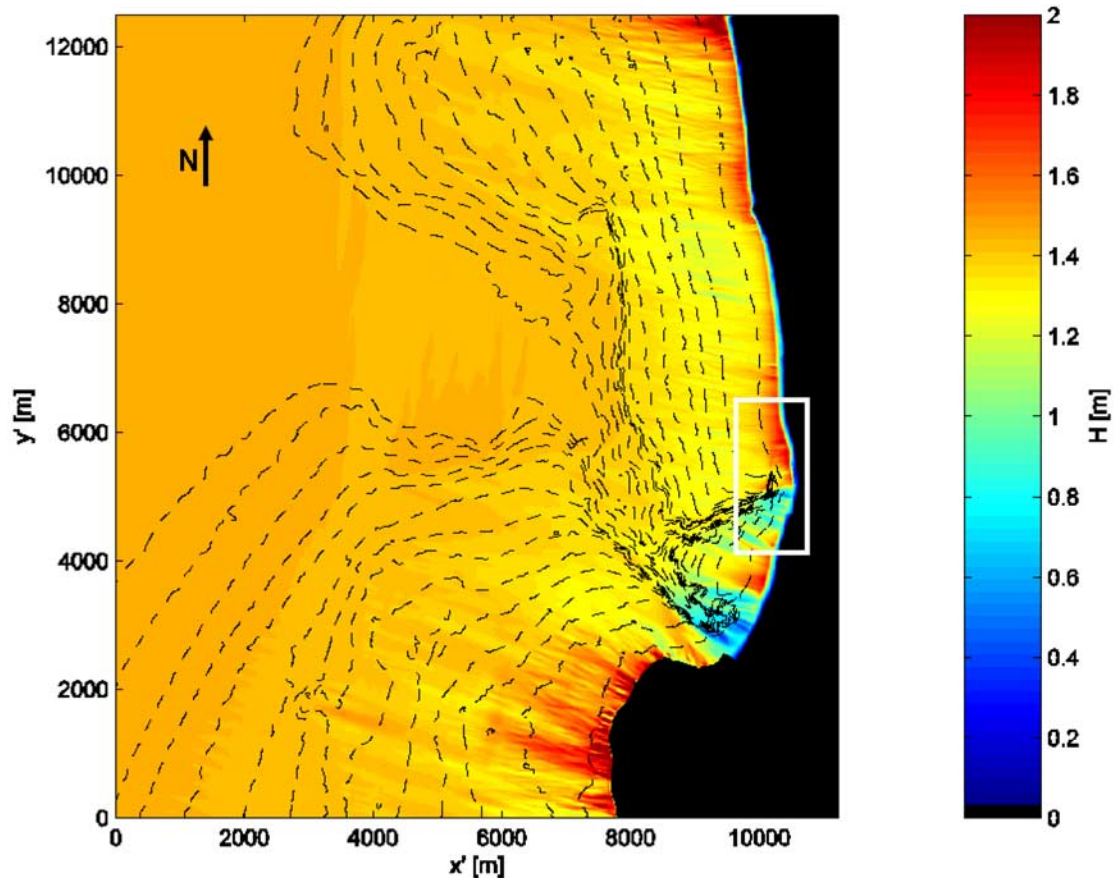

Figure 3. Predicted significant wave height for October 10, 2003 at 1900 GMT. Depth contours are shown in black in 10 m increments from the 0 m to 100 m contours and in 50 m increments from the 100 m to 300 m contours. Highlighted region denotes the circulation model domain.
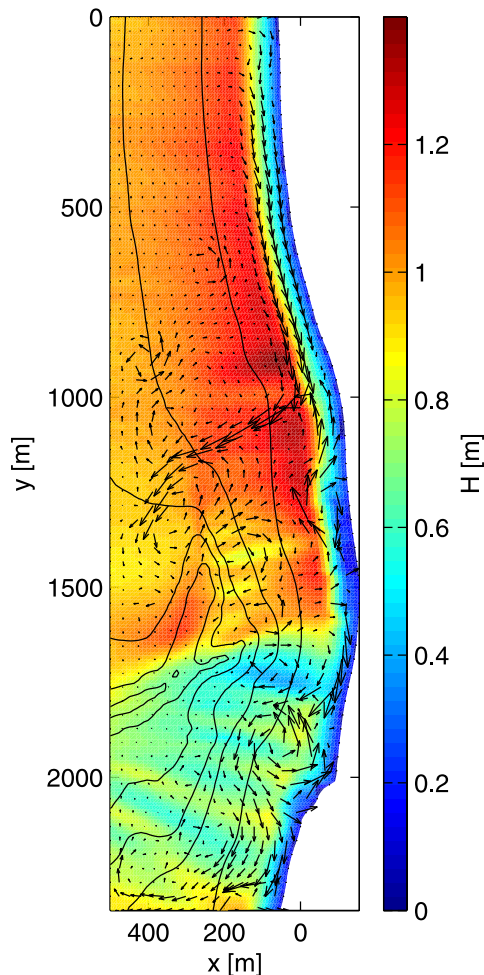
Figure 4. Predicted root-mean-square wave height for October 10, 2003 at 1900 GMT within the circulation model domain (Blacks Beach). Black vectors represent the predicted 10-minute averaged circulation patterns. Depth contours (black) correspond to the 0, 5, 10, 15, 25, 50, and 100 m contours.

that often experiences locally high wave heights caused by a focusing of wave energy north of the canyon. Rip currents are also frequently observed along this section of coast. This portion of the site is characterized by a number of features that may contribute to the observed circulation patterns: a curved shoreline, an oblique canyon stretching towards the nearshore, and undulating canyon contours. Initial circulation modeling efforts presented in this paper have concentrated on this region where extensive data was collected during the experiment.

2.2. Bathymetric Surveys

[6] The site bathymetry was constructed from a series of historical surveys that were first recorded via depth soundings by the National Ocean Service in 1932 and 1972. As technology progressed, updated land elevations were recorded using lidar equipment in 1998, and subsequent surveys of the submarine canyon were performed in 2001 using swath sonar technology. Also in 2001, additional nearshore surveys were conducted via a personal watercraft equipped with a differential global positioning system

(DGPS) to track horizontal position and a sonar altimeter to record elevations with an estimated RMS vertical error of ±5−7 cm [*Smith et al.*, 2003]. An ATV and dolly equipped with a DGPS were used to collect land elevations of the shoreface and overlapping data in the inner surf zone with an estimated horizontal and vertical error in the land surveys of ±1−2 cm and ±2−3 cm, respectively [*Morton et al.*, 1993; *Dail et al.*, 2000]. All pre-experiment data was made available on a map using the most recent data in areas where historical surveys overlapped. This base bathymetry map was updated with each survey conducted during the experiment and the boundary of the survey area was interpolated using a scale-controlled linear interpolation scheme [*Plant et al.*, 2002] to ensure no discontinuities existed. Collectively, numerous NCEX participants used these same procedures to perform biweekly surveys of the shoreface and nearshore bathymetry during the experiment over a 3 km section of shoreline and reaching to approximately the 10 m depth contour. Detailed bathymetric maps corresponding to each survey period were then available to use in the ensuing model simulations.

2.3. Offshore Wave Spectra

[7] The offshore wave climate was measured using a Datawell directional wave buoy deployed by the Coastal Data Information Program, Integrative Oceanography Division, operated by the Scripps Institution of Oceanography. This buoy is located about 11 km offshore of Torrey Pines Beach in a water depth of 550 m and collects wave energy, wave direction, and temperature data. Statistical information and spectral estimates of the water surface elevation are derived from each thirty-minute time series collected by the buoy [*Seymour et al.*, 1985]. The directional wave spectrum from the hour of interest is used to initialize the model series.

2.4. Remote Sensing Observations (Argus)

[8] The Coastal Imaging Laboratory at Oregon State University collected video observations of the nearshore region from an automated Argus video monitoring station situated atop the Southwest Fisheries Science Center on the adjacent cliffs that provided a range of views along Blacks Beach. Video techniques provide clear signals of some physical processes in the surf zone from which geophysical properties can be inferred [e.g., *Holman et al.*, 1993; *Lippmann and Holman*, 1989; *Chickadel et al.*, 2003]. Time exposure images from an average of a series of snapshots collected over 10-minutes allow easy identification of the surf zone by the area of bright intensity due to foam generated through wave breaking. Alternatively, a variance image from the same series of snapshots indicates areas where the surface brightness is fluctuating in time. This is indicative of the swash zone, the outer edge of the surf zone, or time-dependent circulation features such as rip currents. Alongshore locations of observed rip currents can be compared to the model-predicted rip current locations, providing a qualitative indication of the model capabilities.

3. NCEX Model Simulations

[9] The model series used for this research consisted of a spectral wave model to calculate wave transformation and
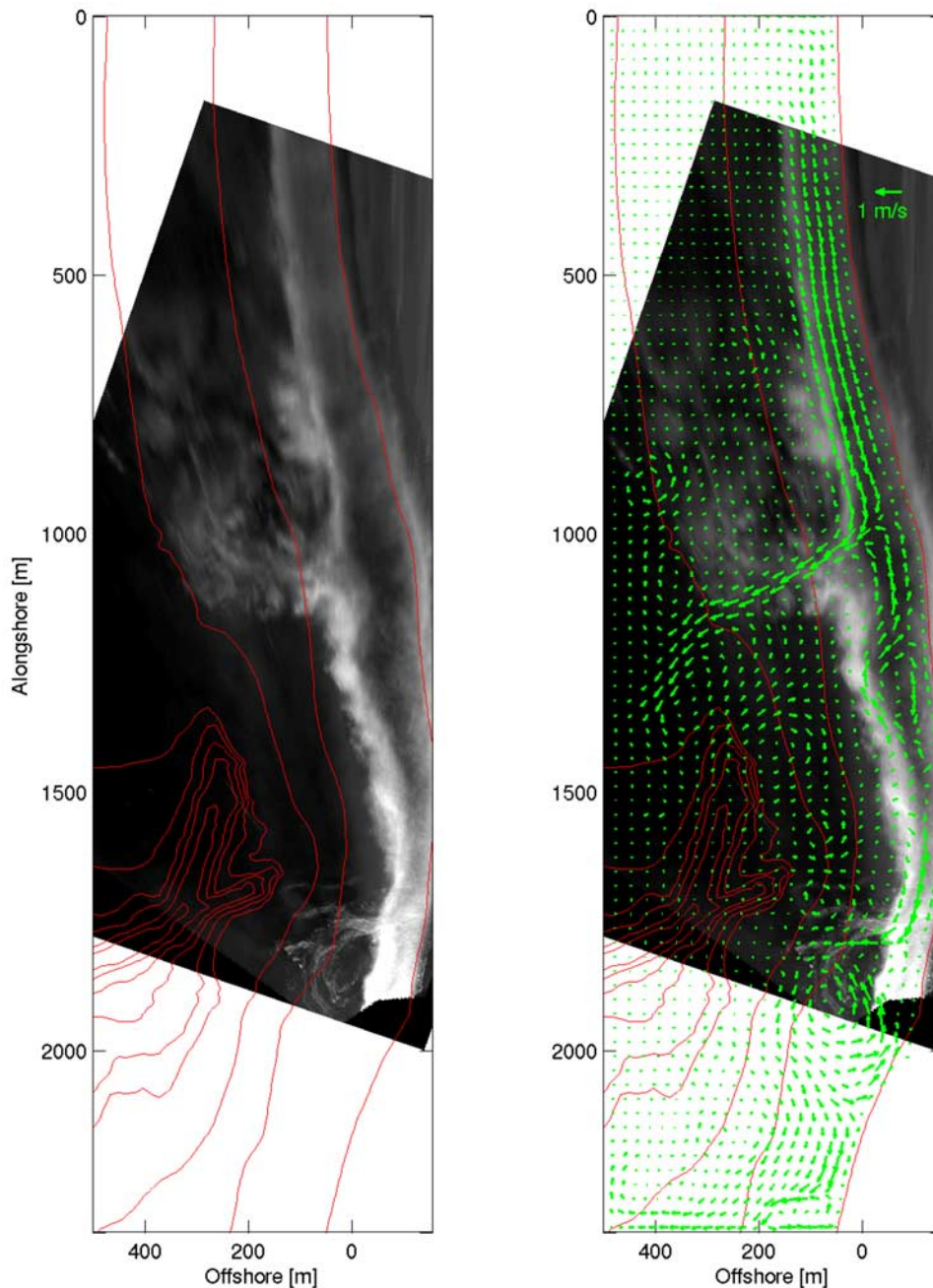
Figure 5. (left) Argus variance image from October 10, 2003 at 1900 GMT. Depth contours (red) correspond to the 0, 5, 10, 20, 25, 35, 50, 75, and 100 m contours. (right) Predicted 10-minute average velocity field at Blacks Beach (green vectors) superimposed on the Argus variance image.

wave forcing (radiation stress gradients). This information was then passed to a nearshore circulation model to calculate a map of wave-driven current velocities.

3.1. Wave Model

[10] The numerical wave model used in this study, the Simulating WAves Nearshore (SWAN) model described by *Booij et al.* [1999], is a spectral wave refraction model that solves the action balance equation and accounts for wave shoaling and refraction as well as depth-induced wave-breaking. The offshore spectrum from the buoy,

representing the main energy source in the system, was used to initialize the model at the offshore and lateral boundaries of the domain. Other processes that may be important in predicting rip currents are wave-current interaction, surface rollers that shift the transfer of momentum from waves to currents shoreward, and wave diffraction, which allows for energy leakage along the wave crest. It is hypothesized, however, that each of these processes only affects the strength or structure of rip currents, not the alongshore position. Therefore each of these has been neglected at this phase and the principal
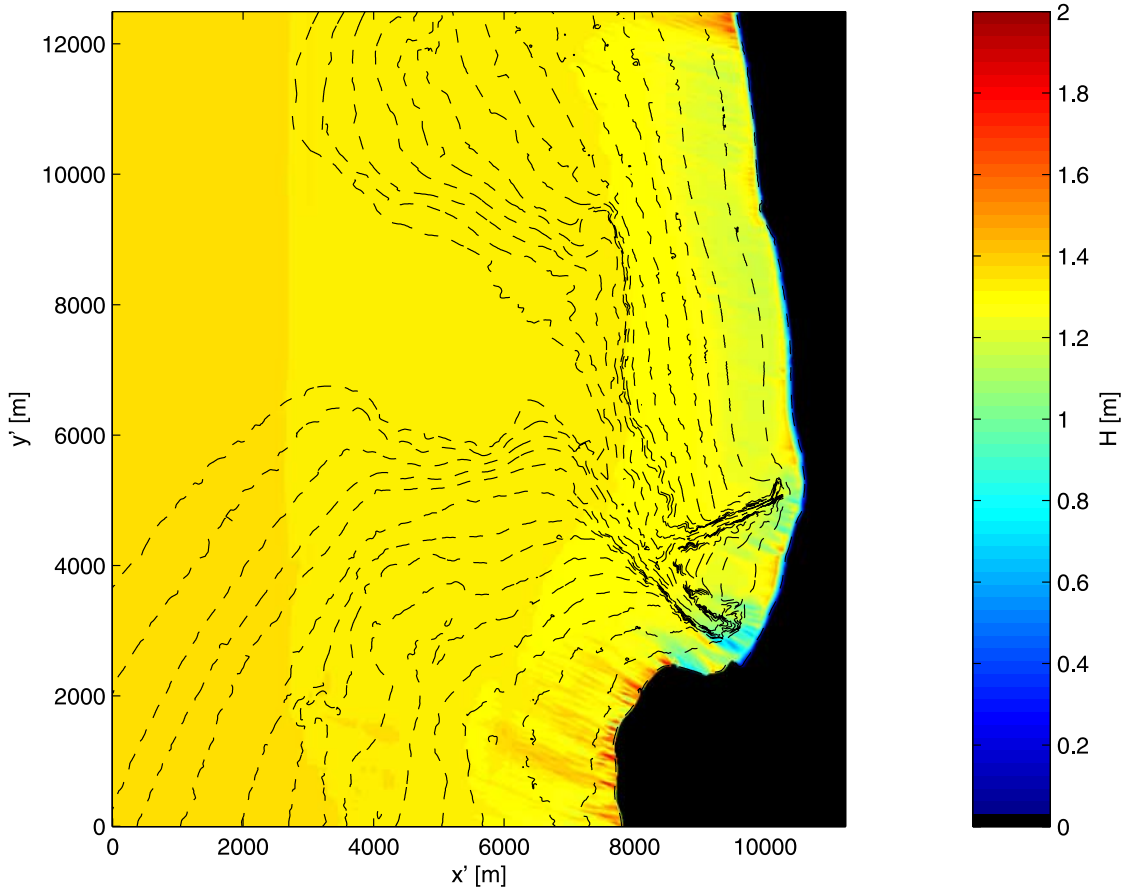
Figure 6. Predicted significant wave height (SWAN) for October 31, 2003 at 1500 GMT. Depth contours are shown in black in 10 m increments from the 0 m to 100 m contours and in 50 m increments from the 100 m to 300 m contours.

diagnostic of the model capability is the accuracy of predicting rip current locations.

3.2. Circulation Model

[11] Radiation stress gradients and bathymetry are provided to the circulation model of *Özkan-Haller and Kirby* [1997, 1999] to obtain two-dimensional horizontal velocity information in the nearshore region. The model solves the continuity equation (1) and the depth-integrated time-averaged Navier Stokes equations to simulate the temporally and spatially varying circulation patterns in this region (2 and 3). In these equations, $\vec{u}$ is the depth-integrated current velocity with cross-shore and alongshore components, u and v, respectively. The current velocity, $\vec{u}$, includes the Eulerian particle velocity ($\vec{u}_E$) and the wave induced drift velocity ($\vec{u}_S$) where $\vec{u}_S = \vec{Q}_w/(h + \eta)$ and $\vec{Q}_w$ is defined as the depth-integrated wave mass flux. Hence, the circulation model equations are:

$$\frac{\partial \eta}{\partial t} + \frac{\partial}{\partial x}[u(h+\eta)] + \frac{\partial}{\partial y}[v(h+\eta)] = 0 \qquad (1)$$

$$\frac{\partial u}{\partial t} + u\frac{\partial u}{\partial x} + v\frac{\partial u}{\partial y} = -g\frac{\partial \eta}{\partial x} + \tilde{\tau}_x + \tau'_x - \tau_{bx} \qquad (2)$$

$$\frac{\partial v}{\partial t} + u\frac{\partial v}{\partial x} + v\frac{\partial v}{\partial y} = -g\frac{\partial \eta}{\partial y} + \tilde{\tau}_y + \tau'_y - \tau_{by}. \qquad (3)$$

$$\vec{u} = \vec{u}_E + \vec{u}_S \qquad (4)$$

[12] In these above expressions, the mean water surface elevation is represented by η, h is the still water depth, $\bar{\bar{\tilde{\tau}}}$ represents the incident wave forcing as derived by *Longuet-Higgins and Stewart* [1964], and $\vec{\tau}'$ is the lateral momentum mixing parameterized using an eddy viscosity formulation where the eddy viscosity is given by $\nu_t = Md(\epsilon_b/\rho)^{1/3}$. The breaking wave dissipation is denoted by ϵ_b, ρ is the water density, $d = h + \eta$, and M is the lateral mixing coefficient [*Battjes*, 1975]. Bottom friction is represented by $\vec{\tau}_b = 2/(\pi d)c_f u_0 \vec{u}$, where u_0 is the amplitude of the horizontal orbital velocity and c_f is the bottom friction coefficient. The two free parameters in the model; the bottom friction coefficient (c_f) and the lateral mixing coefficient (M) were assigned constant values throughout this study with $c_f = 0.003$ and $M = 0.25$. The spatial derivatives in the solution are approximated using a finite difference approach in the alongshore direction and a Chebyshev collocation method in the cross-shore direction. Temporal derivatives are treated using a high order explicit time-integration scheme.
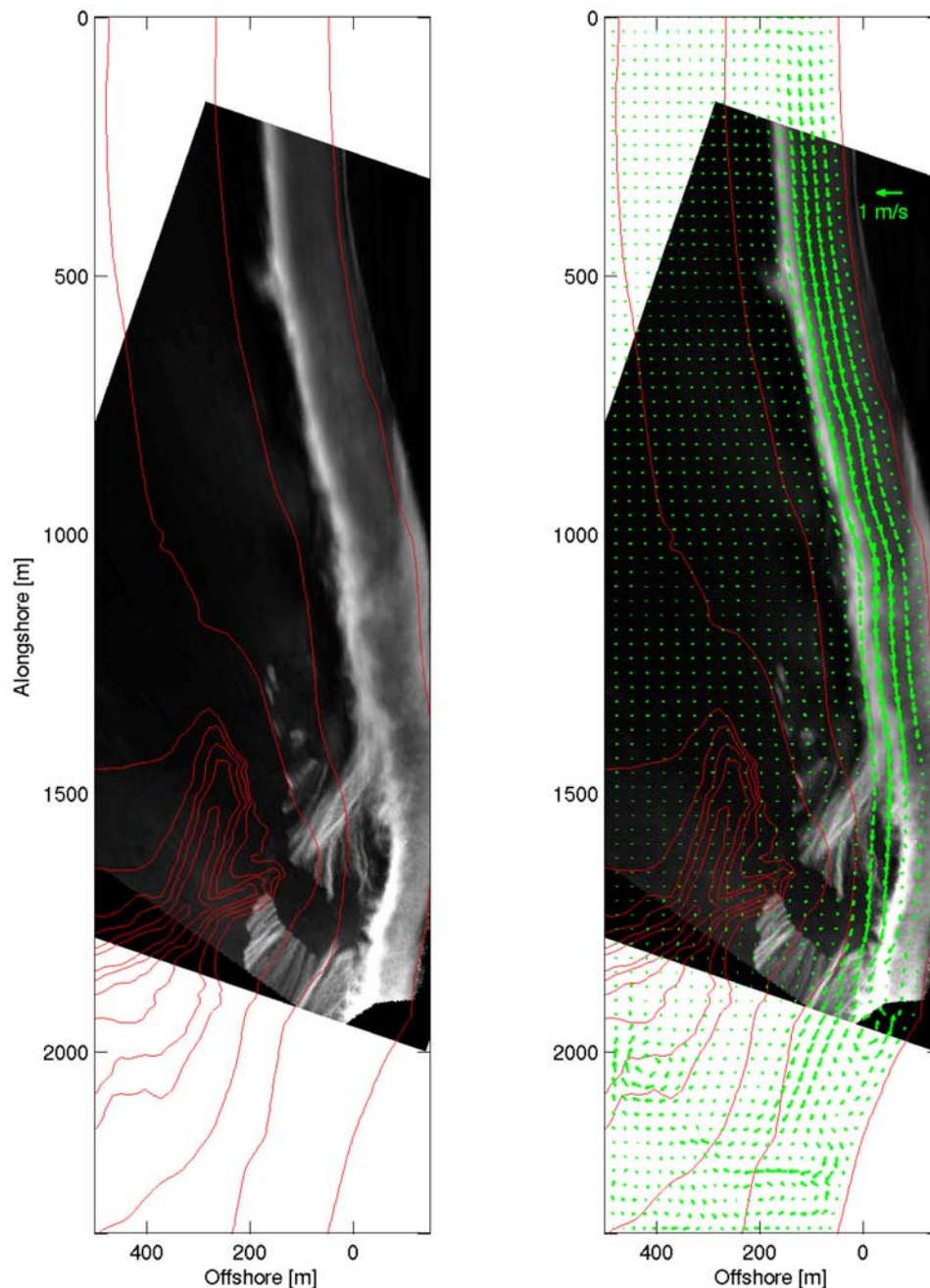
Figure 7. (left) Argus variance image from October 31, 2003 at 1500 GMT. Depth contours (red) correspond to the 0, 5, 10, 20, 25, 35, 50, 75, and 100 m contours. (right) Predicted 10-minute average velocity field at Blacks Beach (green vectors) superimposed on the Argus variance image.

Wall boundaries were defined at the offshore, onshore, and lateral boundaries and wave run-up has been neglected.

3.3. Model-Data Comparisons

[13] A qualitative assessment of the model series was performed by comparing model results to remote-sensing observations for two rip current events. The purpose of this work is not to validate each model individually, therefore detailed evaluations of the wave and circulation models will be addressed in future research efforts. Rather, the following simulations motivated us to further pursue the effects of undulations in the offshore contours in generating nearshore circulation patterns. The wave model domain (see Figure 3) extends 10 km offshore and 12.5 km along the coast of Southern California. The grid consisted of 722 cross-shore nodes with a spacing of 15.58 m and 1350 alongshore locations with a spacing of 9.26 m. The origin of the wave model domain is located offshore and the cross-shore and alongshore coordinates are denoted by x' and y', respectively. For the two model-data comparisons, the spectrum is assumed to be spatially homogeneous and is applied to the offshore as well as lateral boundaries. The water depth at the offshore boundary of the wave model domain was such that wave components with frequencies larger than about
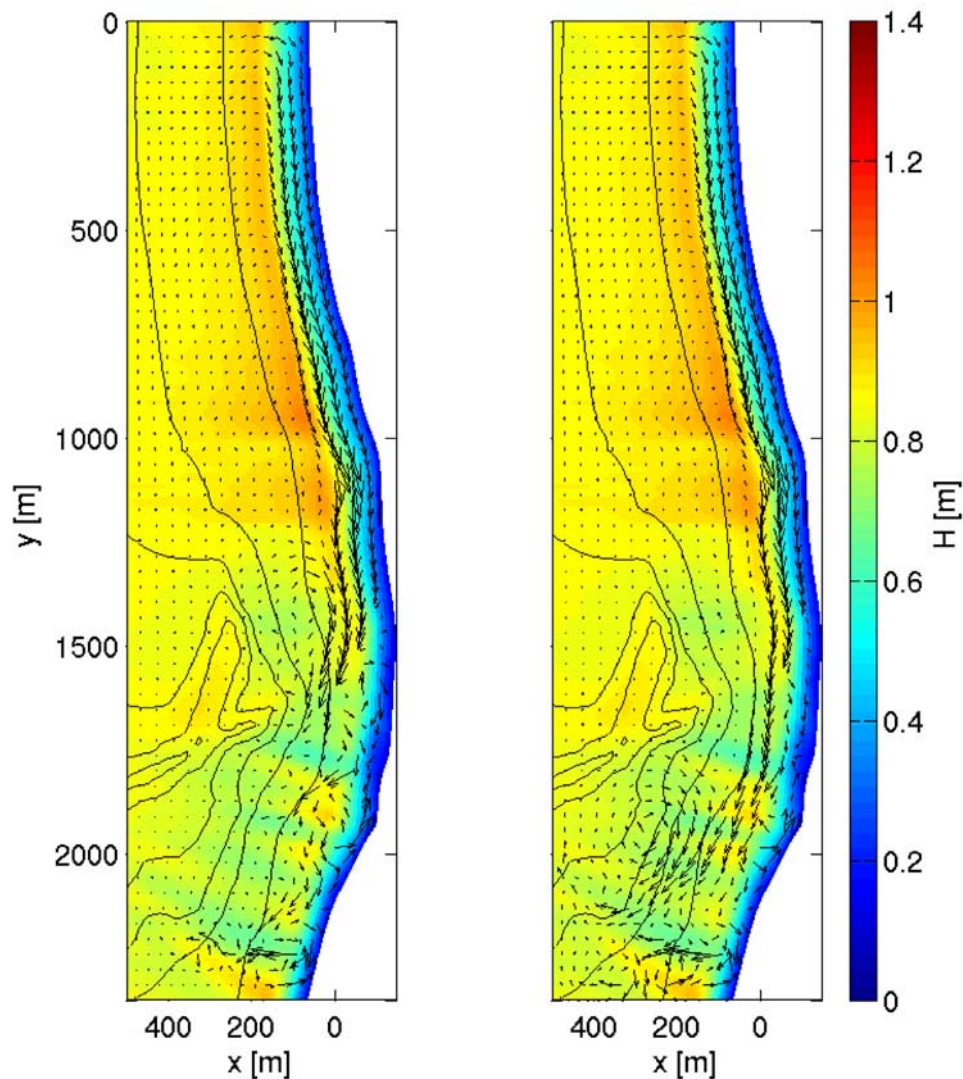
Figure 8. Predicted root-mean-square wave height for October 31, 2003 at 1500 GMT within the circulation model domain (Blacks Beach). Black vectors represent the predicted 10-minute averaged circulation patterns after a 45-minute simulation (left) and a 90-minute simulation (right). Depth contours (black) correspond to the 0, 5, 10, 15, 25, 50, and 100 m contours.

0.06 Hz were in deep water and accounted for at least 90% of the energy for the days of interest. In addition, the alongshore length of the domain was sufficiently large to prevent effects from the lateral boundaries from becoming artifacts in the nested circulation model grid. The resolution of the offshore directional spectrum was 0.01 Hz in frequency with 5 degree directional bins. The accuracy of the directional resolution was tested for 2, 3, 4, and 5 degree bin sizes. Although the structure of the rip currents was altered (e.g. slight changes in orientation of the offshore flow), the predicted rip current location was unaffected. In addition, the required spatial resolution was also tested by nesting a finer nearshore grid in the wave model with a cross-shore and alongshore spacing of 5 m, however there was no change to the predicted rip current location. The circulation model domain (Figure 4), nested inside the larger wave computational domain, is centered along Blacks Beach spanning an alongshore distance of 2.5 km and extends about 500 m offshore.

The circulation grid is 65×257 with variable cross-shore spacing that ranges from 4.56 m to 10.33 m and an alongshore spacing of 9.18 m. The origin here is located on the subaerial beach and the cross-shore coordinate (x) increases offshore and points west while the alongshore coordinate (y) follows a right-handed coordinate system and points south.

3.3.1. Results for October 10, 2003 at 1900 GMT

[14] The first test case was near the beginning of a four-day period (October 9, 2003 to October 12, 2003) where rip currents were observed in the Argus video data. This rip current event was concurrent with a period of increased wave energy recorded at the offshore buoy with significant wave heights exceeding 1 m. The base bathymetry was updated using survey data collected from October 6th and October 7th, and spectral estimates of the significant wave height, peak wave period, and peak wave direction at the offshore wave buoy yielded 1.6 m, 10 s, and 282 degrees (waves approaching from the northwest at a 12 degree
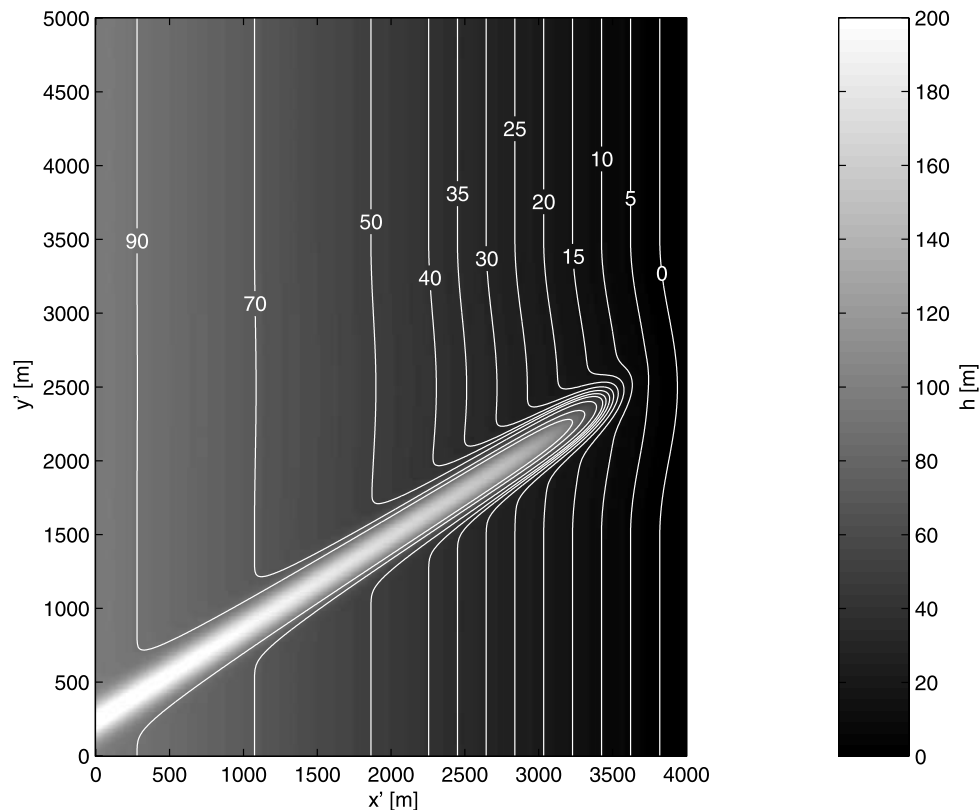
Figure 9. Bathymetry for the theoretical evaluation of rip current development due to an oblique canyon and curved shoreline.

incident angle with respect to the x'-axis), respectively. In addition, there was a secondary peak consisting of wave energy approaching from the south with a peak period of 14 s (Figure 2). The predicted significant wave height variation over the model domain is shown in Figure 3, with the rectangle outlining the boundary of the nested circulation domain. Two predominant length scales of alongshore gradients in the wave height are evident in this region. The large length scale variations (O(km)) occur due to ray divergence over the offshore canyon, with an overall low wave height immediately shoreward of the canyon tips and prevailing areas of increased wave height on either side. There are also shorter length scale variations (O(100 m)) arising from the undulations in the canyon walls. A wave forcing that smoothly increases from zero to the values dictated by the wave model over approximately 50 wave periods (~8 minutes) is used throughout the 1-hr simulation of the wave-induced circulation. The simulation length was chosen to achieve time-invariant rip current locations. For this case, the computed circulation is averaged over the last 10 minutes of the simulation and compared to the variance image derived from a 10-minute average of Argus observations. The resulting circulation field is superimposed on the root-mean-square wave height predictions obtained from the wave model in Figure 4. Rip currents develop in regions of locally low wave height caused by the undulations in the offshore canyon bathymetry at approximately $y = 1000$ m and $y = 1800$ m, as well as in a region of generally high wave height just north of the canyon head. Figure 5 shows the mean velocity vectors, superimposed

on the Argus variance image for this hour. We note here that the predicted rip current locations for this simulation were not influenced by changes in the averaging period. These results provide encouraging agreement between the modeled and observed rip current locations and the evaluation of the survey data reveals no evidence to suggest that the nearshore bathymetry dictates the alongshore position of the concentrated offshore flow.

3.3.2. Results for October 31, 2003 at 1500 GMT

[15] The second test case was chosen at the beginning of another observed rip current event where increased wave energy with significant wave heights over 1 m were recorded at the offshore buoy, however the increase in wave activity as well as surface signatures of the rip currents only persisted for one day. The rip currents observed from the video data collected by various institutions on this day are more difficult to interpret due to the spatial and temporal variability of the surface foam patterns. The series of snapshots collected during this period only provide intermittent signals of rip currents that do not appear for long periods of time or in one specific location. In addition, the observations show that the direction of the offshore flow was much more oblique. The offshore spectrum shown in Figure 2 was bi-modal with a significant wave height of 1.5 m, 6.7 s peak period, and 293-degree peak incident wave direction (waves approaching from the northwest at a 23-degree incident angle with respect to the x'-axis). Compared to the wave climate on October 10th the incident waves were shorter and more oblique but the secondary peaks in both cases were comparable. The bathymetry file was updated using a
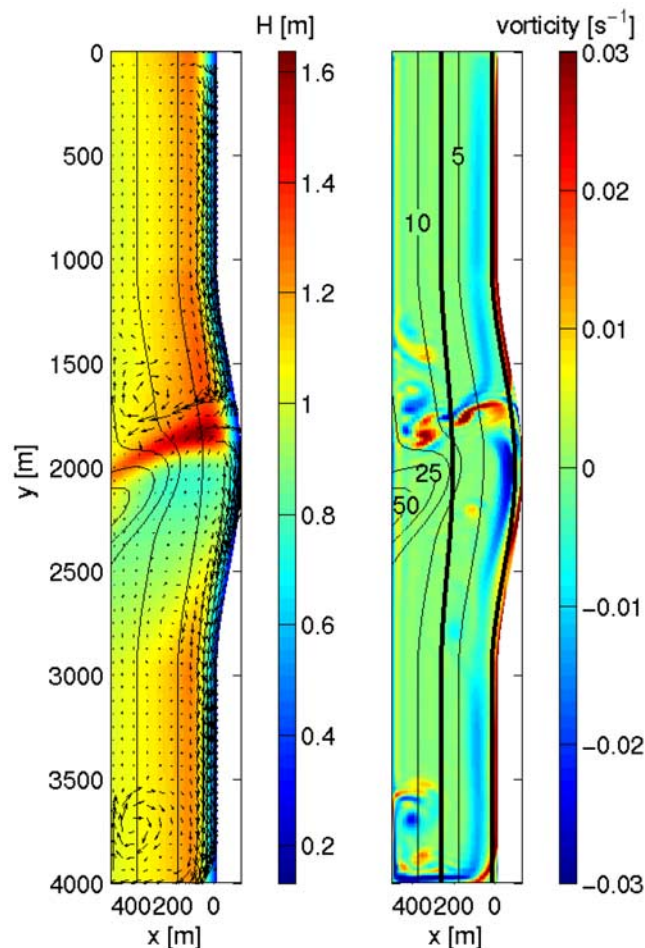
Figure 10. Predicted root-mean-square wave height variation (left) and final snapshot of vorticity (right) for the theoretical case described by an oblique canyon and curved shoreline. Thick black lines in the right panel indicate the transects where the alongshore momentum balances will be evaluated as discussed in section 4.2.

survey conducted on October 27th. For this test case, the same modeling procedure described above was used but the length of the circulation simulation was increased to 90 minutes in order to achieve time invariant rip current locations. The results from the wave model over the entire domain are shown in Figure 6. The predicted significant wave height, plotted using the same color scale as the previous case, indicates that the wave focusing is less pronounced given the conditions on this day. As shown in Figure 7, the northern rip current observed and predicted on October 10th is no longer present, however rip currents are observed in the Argus image at $y = 1500$ m and $y = 1800$ m. The model does not predict the rip current at $y = 1500$ m and provides only a weak signature of the southernmost rip current. The circulation results in this case are very sensitive to the length of the simulation. Shorter simulations produce average velocities that indicate much stronger evidence of rip currents in the locations where they are observed. Figure 8 shows the 10-minute time-averaged circulation vectors superimposed on the wave height variations for an average taken from 35–45 minutes and 80–90 minutes.

With increasing simulation time, the inertia of the strong alongshore current weakens the predicted rip current signature. For instance, a slight offshore flow is predicted after a 45-minute simulation at $y = 1650$ m with more pronounced rip currents around $y = 1900$ m and $y = 2350$ m, which correspond to the currents observed in the Argus variance image. The signature of the northernmost rip, however, is decreased by the end of the 90-minute simulation although there is still some indication of offshore flow at the appropriate locations and an alongshore current at the northern end of the site, which is consistent with the variance image. In the comparisons for both days, the rip currents appear to be related to the shorter length scale variations in the wave field, indicating that these offshore flows can appear in both areas of generally high or generally low wave energy. A series of tests, based on conditions that were different between the two cases, were performed to isolate the mechanism that was responsible for the shift in rip current location that was observed. There were four characteristics identified to vary between the test cases; nearshore bathymetry, wave energy, peak period, and peak wave direction. Changing only a single characteristic at a time, the measured bathymetry used for October 10th was replaced by the bathymetry for October 31st and the model indicated no change in the circulation patterns. This is further evidence that the local nearshore bathymetry is not controlling the development or placement of the observed rip currents. To evaluate the effects of the minor change in offshore wave energy, the integrated energy of the spectrum from October 10th was decreased to correspond to the energy observed on October 31st. Again the model indicated no change in the predicted rip current locations. Although consistent between the two cases, tests performed by removing the energy contained in the southern peak of the spectrum also yielded no change in the circulation patterns. The final characteristics, wave period and wave direction, were also tested and appear to largely contribute to dictating rip current location. Their effects will be examined further in section 4.3.

4. Idealized Bathymetry

[16] At a particular site, isolating the individual feature that is dominant in prescribing the location where rip currents will appear can be impossible due to the complexity of the site bathymetry. As a viable alternative, numerical studies that test each individual relevant characteristic will be provided in this section. The three characteristics that were isolated include an offshore oblique submarine canyon, a curved shoreline positioned near the tip of the canyon, and the presence of undulating features along the canyon walls. The reader is referred to Appendix A for the equations that describe each characteristic bathymetry. Again, the simulation lengths were chosen to achieve time-invariant rip current locations and to ensure that any initial start-up transients had adequate time to propagate to the lateral boundary and would not affect the time-averaged circulation results. For the following cases, 90-minute simulations were performed and the velocity fields and momentum balances were averaged over the last fifteen minutes. A JONSWAP spectrum, described by *Hasselman et al.* [1973], with a 10 s peak period and 285 degree peak direction was used to
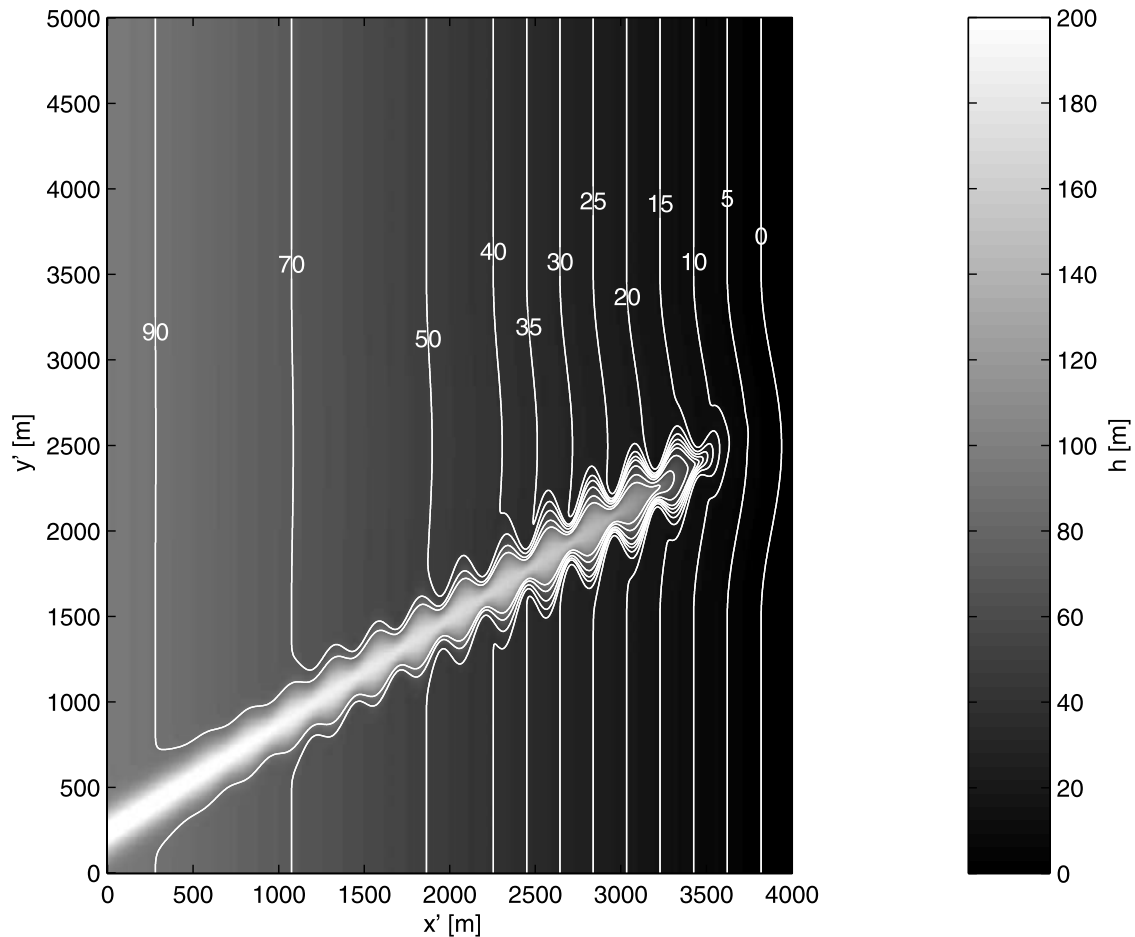
Figure 11. Bathymetry for the theoretical evaluation of rip current development due to an oblique canyon with undulating contours and a curved shoreline.

initialize the model. The spectral shape was chosen to match the narrow-banded primary peak of the measured spectrum from October 10, 2003 at 1900 GMT during the NCEX experiment. The width of the spectrum in frequency was dictated by the peak enhancement factor (γ) of 10 (half power band width of 0.0131Hz) and the directional spread was prescribed using $\cos^m(\theta - \theta_{peak})$; where $m = 40$ (half power directional width of 24.76 degrees). The effects of both normal and obliquely incident spectra over these idealized bathymetries were tested, however for brevity, not all tests will be shown.

4.1. Wave Height and Circulation Results
4.1.1. Smooth Oblique Submarine Canyon
[17] An irregular offshore bathymetry was developed by superimposing a planar beach, sinusoidal shoreline with a contour curvature that dampens with increasing water depth, and an elliptical canyon with the canyon tip positioned near the concave portion of the shoreline (see Figure 9). The wave model grid consists of 801 cross-shore points and 1001 alongshore points with a spacing of 5 m in both directions and the circulation model grid is 65×512 with a variable cross-shore spacing of 0.1 m to 15.92 m and an alongshore spacing of 7.8 m. The predicted wave height patterns along with the time-averaged circulation field at the end of the simulation and final snapshot of vorticity are

shown in Figure 10. There is a region of intense wave focusing just above the canyon tip, similar to that predicted at the NCEX site. In this case, one rip current developed up-current of the region of increased wave height where the alongshore current in the negative y-direction driven by the pressure gradient collides with the alongshore current in the positive y-direction generated by obliquely breaking waves that are unaffected by the submarine canyon. No rip current developed down-current of the canyon. The wall boundaries prescribed at the ends of the domain are apparent in the results, however it is noted that these effects are localized at the lateral boundaries and do not affect the rip current location or structure.

4.1.2. Undulating Oblique Submarine Canyon
[18] The following case involved including undulations with a characteristic length scale of 100 m in the canyon contours as shown in Figure 11. As indicated by the predicted wave height in Figure 12, these features significantly alter the nearshore wave field creating alongshore variations with length scales similar to the sinusoidal canyon variations. The rip current at around $y = 1700$ m still exists but additional rip currents are predicted within these variations, particularly in areas of intermediate wave height. The results show that during the simulation some vortices emitted from the rip currents reach and reflect from the offshore boundary. Simulations using twice the cross-
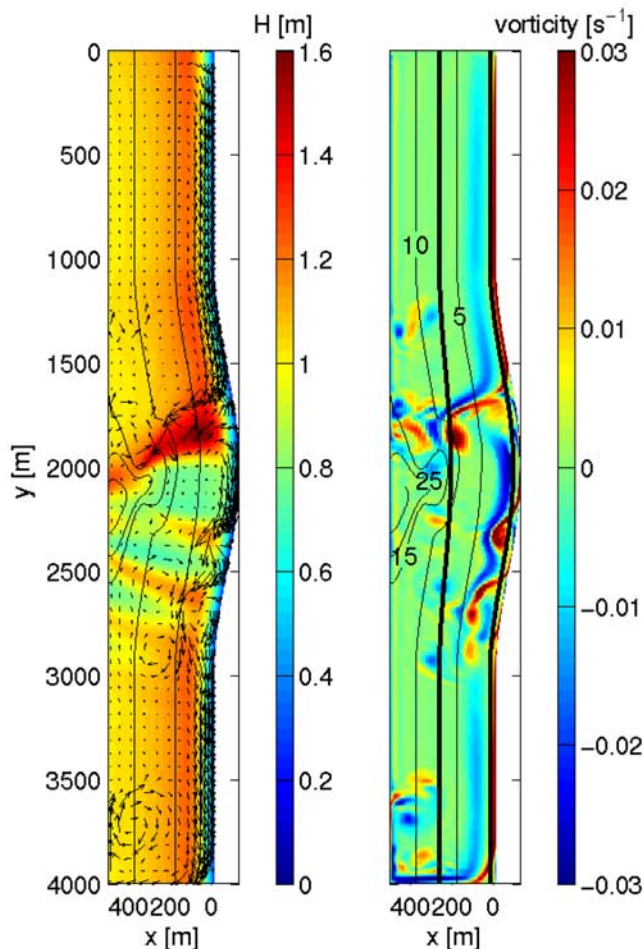
Figure 12. Predicted root-mean-square wave height variation (left) and final snapshot of vorticity (right) for the theoretical case described by an oblique canyon with undulating contours and curved shoreline. Thick black lines in the right panel indicate the transects where the alongshore momentum balances will be evaluated as discussed in section 4.2.

shore domain length have been performed while retaining the cross-shore resolution, and results indicate that rip current locations and magnitudes are not affected by the interaction of emitted vortices with the offshore boundary. Hence, the results for this idealized case show that features in the offshore bathymetry can be the controlling factor in rip current development and location.

4.2. Time-Averaged Momentum Balances

[19] The previous discussion focused on the site characteristics that may be dominant in dictating rip current location; however, evaluating the alongshore variability of the forcing generated by these characteristics can further enhance our understanding of what controls the locations where rip currents are likely to develop. Within the circulation model, a physical grid that includes a curved shoreline is transformed to a computational grid as discussed in detail by Özkan-Haller and Kirby [1999]. To evaluate locally orthogonal alongshore momentum balances and understand the governing balance, it is imperative

to translate the model output vectors in the (x,y)-coordinate system to a system that is locally orthogonal to the physical grid. The details of this transformation are provided in Appendix B. In this section, the time-averaged alongshore momentum balances inside and outside the surf zone will be presented for the aforementioned idealized cases. The transect locations correspond to the lines in the vorticity results previously shown in Figures 10 and 12.

4.2.1. Smooth Oblique Submarine Canyon

[20] The time-averaged momentum balances were evaluated at a number of time intervals to examine the time evolution of the force balance and resulting rip current locations. The most intuitive balance appears after three minutes of simulation time, before nonlinearities in the system begin to arise. Based on the study of Bowen [1969], the alongshore momentum balance offshore of wave breaking should consist of the alongshore pressure gradient and opposing wave forcing. These components should exactly balance so no net forcing of circulation is present offshore of the breaking location. Inside of the surf zone, however, the balance is expected to be between the alongshore pressure gradient and the bottom friction. The 3-minute time-averaged alongshore momentum balances inside and outside the surf zone for the smooth oblique canyon case are shown in Figure 13. Each forcing term from the momentum balance equation (B1) is indicated, including the time-averaged acceleration of the alongshore current. Positive values of the radiation stress forcing and wave-induced setup in Figure 13 drive currents in the positive y-direction and the bottom friction is indicative of the alongshore current where a negative friction represents a positive alongshore current. Finally, a positive local acceleration of the current illustrates an acceleration of the flow in the positive y-direction. Outside of the surf zone there is a balance between the gradient in the mean water surface elevation and the incident wave forcing, consistent with the results of Bowen [1969] (Figure 13, top panel). At the beginning of the simulation the balance is not exact due to flow accelerations that exist. Inside the surf zone there is an imbalance between the pressure gradient and the incident wave forcing, which results in a strong acceleration of the alongshore current (bottom panel). Although, in general, the direction of the incident waves force a positive alongshore current, in the region where the waves refract due to the underlying canyon, the wave forcing acts in the opposite direction (1700 m < y < 2000 m). The alongshore momentum balances resulting from averaging over the last 15 minutes of the simulation are shown in Figure 14 and indicate that nonlinear aspects of the nearshore circulation become quite important as the simulation continues. In particular, it is apparent that outside of the surf zone, the balance in the vicinity of the rip current (1500 m < y < 1700 m) is primarily between the pressure gradient and the competing nonlinear acceleration terms, however the balance away from the narrow rip current jet has remained the same. Note that the rip current extends outside of the surf zone and nonlinearity is therefore evident in the offshore momentum balance. For the surf zone transect, the dominant balance resembles the offshore balance within the rip current circulation cell, however, away from this region (y < 1350 m & y > 3000 m), it reverts to the expected balance between the wave forcing and bottom
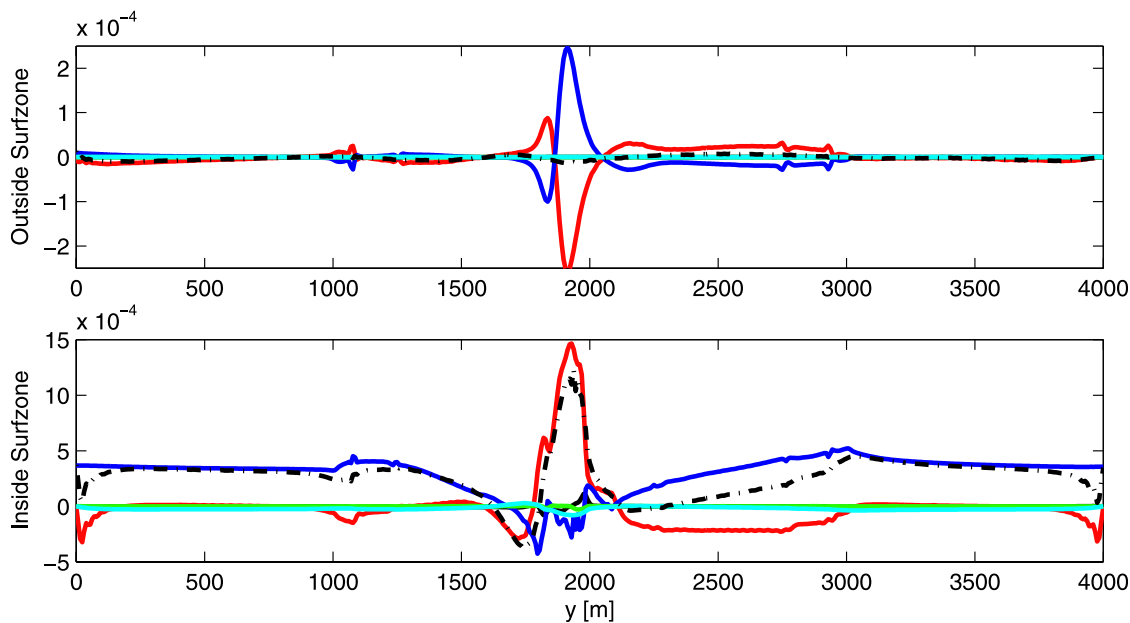
Figure 13. Smooth Oblique Submarine Canyon: Time-averaged alongshore momentum balances outside the surf zone (top) and inside the surf zone (bottom) after 3 minutes of simulation length; $\left\langle \frac{\partial v}{\partial t} \right\rangle$ (black dashed), $\left\langle \overline{u\frac{\partial v}{\partial x} + v\frac{\partial v}{\partial y}} \right\rangle$ (black solid), $\left\langle \overline{g\frac{\partial \eta}{\partial y}} \right\rangle$ (red), $\left\langle \overline{\tau_y} \right\rangle$ (blue), $\left\langle \overline{\tau'_y} \right\rangle$ (green), $\left\langle \overline{\tau_{by}} \right\rangle$ (cyan).

friction. The portions of the transect within 500 m of the lateral boundaries are clearly affected by the wall boundary condition as indicated by large advective accelerations; however the effects are localized to the vicinity of the boundaries. The advective acceleration terms return to near zero for an additional 500 m towards the interior of the domain indicating that the choice of boundary condition will not affect the momentum balances in the vicinity of the rip currents. In the bottom panel of Figure 14, the effect of nonlinearity is reinforced through a comparison of the predicted mean cross-shore velocity at the approximated breaking location for the nonlinear model simulation discussed so far and a simulation using linearized model equations. Positive values of cross-shore flow indicate offshore directed currents exiting the surf zone. The linear simulation, lacking spatial acceleration, predicts rip currents at approximately $y = 1690$ m and $y = 1950$ m while the nonlinear model predicts only the rip current north of the canyon at $y = 1680$ m. There is a slight 10 m shift in the rip current location and a narrowing of the rip current jet associated with nonlinearity. It is noted that the nonlinear model also predicts a rip current around $y = 1950$ m at the start of the simulation, however the inertia of the strong positive alongshore current quickly sweeps away the rip current. Although not discussed in detail, we have also performed simulations for the case of a straight shoreline with a submarine canyon and a curved shoreline with no submarine canyon. For the former case, only one rip current developed up-current of the canyon due to the convergence of the alongshore current associated with the obliquely breaking waves and the opposing pressure-driven current associated with the wave focusing region at $y = 1800$ m. The curved shoreline with no submarine canyon resulted in

regions of wave focusing on either side of the shoreline embayment that were of smaller magnitude than the pressure gradient caused by the presence of a canyon. The alongshore current in the positive y-direction due to the oblique waves was reinforced by the pressure gradient up-current of the embayment. However, the inertia of the alongshore current could not overcome the opposing pressure gradient down-current of the concave shoreline resulting in a rip current at $y = 2200$ m. The addition of an oblique canyon causes a marked increase in the pressure gradient up-current of the canyon, resulting in a stronger alongshore current traveling in the positive alongshore direction with sufficient inertia to overcome the opposing pressure gradient it encounters as it propagates out of the embayed shoreline region ($y = 2750$ m). As the alongshore current reaches the point of maximum wave height following the shadow region ($y = 3000$ m), it was reinforced by the positive incident wave forcing. In summary, for the case of a straight shoreline and a submarine canyon, one rip current develops up-current of the canyon as the pressure-driven flow collides with the alongshore current driven by the obliquely breaking waves. In the case of only a curved shoreline one rip current at the down-current side of the embayment is formed due to the curvature of the shoreline. The linear superposition of these two bathymetries does not result in two rip currents as may be expected. Instead the rip current caused by the embayment is no longer present because it is overpowered by the inertia of the pressure gradient-driven flow associated with the wave focusing induced by the canyon.

4.2.2. Undulating Oblique Submarine Canyon

[21] The momentum balances become somewhat more complicated as the undulations in the canyon walls are
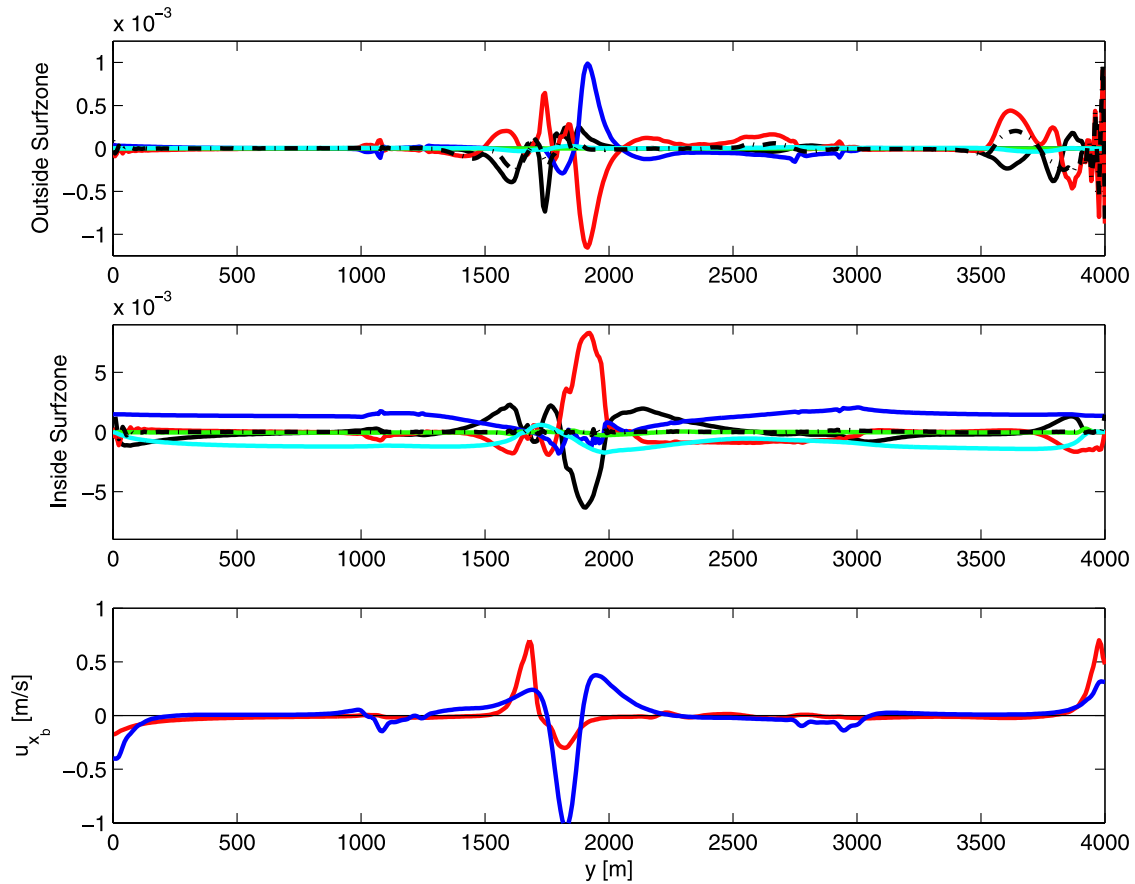
Figure 14. Smooth Oblique Submarine Canyon: Time-averaged alongshore momentum balances outside the surf zone (top) and inside the surf zone (middle), averaged over the last 15 minutes of the 90-minute simulation; $\left\langle \frac{\partial v}{\partial t} \right\rangle$ (black dashed), $\left\langle u\frac{\partial v}{\partial x} + v\frac{\partial v}{\partial y} \right\rangle$ (black solid), $\left\langle g\frac{\partial \eta}{\partial y} \right\rangle$ (red), $\left\langle \widetilde{\tau_y} \right\rangle$ (blue), $\left\langle \overline{\tau'_y} \right\rangle$ (green), $\left\langle \overline{\tau_{by}} \right\rangle$ (cyan). (bottom) Time-averaged cross-shore velocity at the approximated breaking location for the linear model (blue) and the nonlinear model (red).

included, however they are still consistent with the principles discussed for the previous cases. The alongshore momentum balances resulting from the last 15 minutes of the simulation are provided in Figure 15. Although multiple rip currents are present, the change in rip current location due to nonlinearity, and a dominant balance between the gradient in the mean water surface and the advective acceleration components inside the current are still evident. The rip current above the canyon ($y = 1700$ m) is predicted regardless of the inclusion of nonlinearity, and the width of the rip current predicted in linear model is reduced by 50% in the nonlinear simulation. Similar to the smooth canyon case, the rip current in the shadow region of the canyon at $y = 1950$ m is predicted by the linear model only. Rip currents associated with the O(100m) undulations are present in both simulations but the inertial effects included in the nonlinear model shift the alongshore position of the rip currents south between 50 and 80 m. We note that the locations of rip currents in the linear model are at local minima in the wave height, where the sum of the alongshore pressure gradient and incident wave forcing is zero. In contrast, rip currents in the nonlinear model are shifted to areas of intermediate wave height by inertial effects, which is

consistent with the early observations of *Shepard and Inman* [1950].

4.3. Effects of Varying Spectral Parameters

[22] The refraction patterns of waves propagating over bathymetric features are highly dependent on the incident wave parameters. Consequently, the nearshore circulation patterns, including rip current locations, are also affected by changes to the offshore wave spectra. To evaluate the responsiveness of the rip current locations to changes in the incident wave field, four parameters of the offshore wave spectrum were varied; the peak incident wave period and direction, and the widths of the frequency and directional peaks. Using the undulating canyon as the characteristic bathymetry, the results of these tests are discussed in the following sections.

4.3.1. Peak Incident Period

[23] The effect of changes to the spectral peak period on the wave refraction patterns can be significant, even with variations of only $1-2$ s. Numerous tests were performed varying the peak period from 6 to 14 s in increments of 2 s. The results from three of the cases, corresponding to a peak period of 6, 10, and 14 s are shown in Figure 16 to illustrate
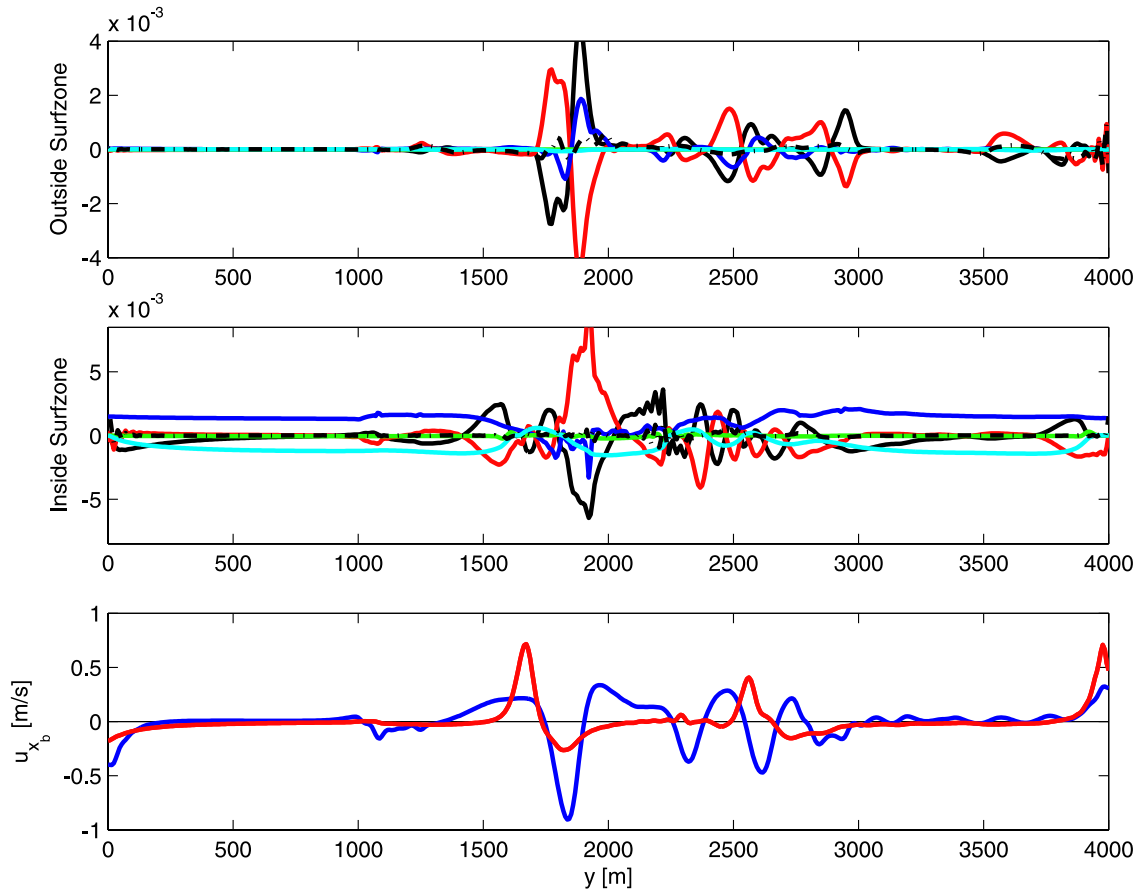
Figure 15. Undulating Oblique Submarine Canyon: Time-averaged alongshore momentum balances outside the surf zone (top) and inside the surf zone (middle), averaged over the last 15 minutes of the 90-minute simulation; $\left\langle \frac{\partial \bar{v}}{\partial t} \right\rangle$ (black dashed), $\left\langle \overline{u\frac{\partial v}{\partial x} + v\frac{\partial v}{\partial y}} \right\rangle$ (black solid), $\left\langle \overline{g\frac{\partial \eta}{\partial y}} \right\rangle$ (red), $\left\langle \overline{\tau_y} \right\rangle$ (blue), $\left\langle \overline{\tau'_y} \right\rangle$ (green), $\left\langle \overline{\tau_{by}} \right\rangle$ (cyan). (bottom) Time-averaged cross-shore velocity at the approximated breaking location for the linear model (blue) and the nonlinear model (red).

the range of predicted changes. The simulated mean circulation field is superimposed on the wave height predictions to illustrate the flow patterns and rip current locations. The figures indicate that shorter waves are less affected by the presence of the canyon. Conversely, longer waves experience stronger refraction of the wave crest resulting in larger alongshore wave height gradients. The same is true for wave transformation caused by the undulations in the canyon walls. Although the length scale of the wave height variations does not change, the magnitude of the wave height gradient will. In cases where shorter waves are present, the pressure gradient may not be large enough to force alongshore currents of sufficient strength, and the currents forced by obliquely breaking waves become dominant, creating a nearly uniform alongshore current. These results are consistent with the observations of *Shepard and Inman* [1950], which indicated that longer waves generated stronger regions of wave convergence that, in turn, resulted in well-defined and stable rip currents. Alternatively, when shorter waves were present at this site, they found that the alongshore current direction was dictated by the direction of the incident waves and the circulation cells were highly variable in time.

4.3.2. Frequency Distribution

[24] The response to variations in the width of the frequency spectra was investigated while maintaining a constant spectral energy, peak period and peak direction. For these simulations, the width of the JONSWAP spectrum in frequency was prescribed by the parameter gamma, γ, which was defined as 1, 3.3, 10, and 20 resulting in successively narrower spectra with a half power width of the frequency peak of about 0.058 Hz, 0.020 Hz, 0.013 Hz, and 0.011 Hz, respectively. Although not shown here, there were only minor differences in the wave height intensity between the simulations and no significant changes to the nearshore circulation patterns were recorded.

4.3.3. Peak Direction

[25] The responsiveness of the rip current location to changes in peak incident wave direction was evaluated using a procedure similar to that in section 4.3.1. In this instance all spectral parameters remained constant, except for the peak direction which was modified from 270 degrees (normally incident) to 315 degrees (waves approaching from the northwest at 45 degrees) in increments of 15 degrees. The results representing the range of conditions (270 degrees, 285 degrees, and 315 degrees) are provided in Figure 17.
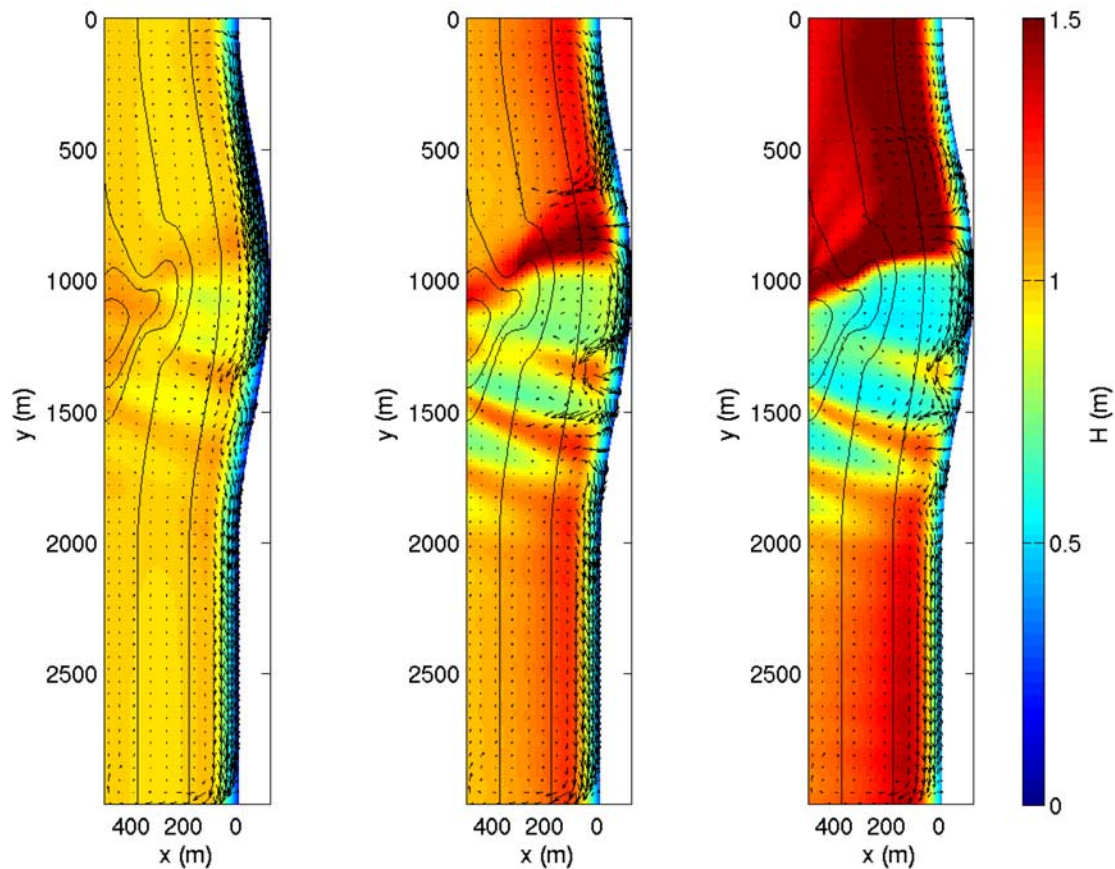
Figure 16. Predicted velocity field (black vectors) superimposed on the predicted root-mean-square wave height for the following wave conditions: JONSWAP spectrum with Hs = 1.5 m, θ_p = 285 degrees, γ = 10, m = 40, and (left) T_p = 6s, (middle) T_p = 10s, (right) T_p = 14s. Depth contours (black) correspond to the 0, 5, 10, 15, 25, and 50 m contours.

Interestingly, these results show that the peak incident direction can have a considerable effect on the rip current location by altering the refraction pattern over the canyon undulations. For instance, normally incident waves provide a more intense region of wave focusing north of the canyon tip, although the smaller length scale variations are less intense and may not extend into the nearshore region where currents are generated. As the incident angle becomes more oblique, the wave focusing region north of the canyon is weakened, but the influence of the undulations becomes more pronounced. These changes can result in a southward shift of the circulation patterns (O(50 m)) and/or the development of additional rip currents. However, it is a delicate balance, because as the incident wave angle increases to 315 degrees, the alongshore current becomes so strong that its inertia overpowers the alongshore pressure gradients and no rip currents are generated.

4.3.4. Directional Distribution

[26] Finally, tests were performed to consider the width of the incident spectra in wave direction. The power, m, was assigned values ranging from 4 to 200 where an increase constitutes a narrowing of the energy spectrum. Figure 18 provides the wave and circulation fields corresponding to an offshore spectra where m = 4, 24, and 40 (half power width of the directional peak of 65.71, 27.88, and 24.76 degrees, respectively). A narrowly distributed spectra results in a

well-defined alongshore wave height variations associated with the undulating canyon walls and pressure gradients sufficient to induce rip currents. Broadening of the spectra begins to smooth the variations which causes an alongshore shift of the rip current positions. A further increase in the directional spread of the spectra will continue to decrease of the magnitude of pressure gradient. This reduction eventually results in a situation where the wave height variations associated with the undulations are not sufficient to cause rip currents to develop. This is illustrated in Figure 18 for the simulation with the broadest directional spread (m = 4), where the rip current that developed near y = 600 m in previous simulations is no longer present.

5. Discussion

[27] In this study, we have considered the depth-averaged circulation field generated by waves that shoal, refract and break over a bathymetry that includes offshore submarine canyons. We reiterate here that we have not accounted for the effects of wave diffraction. We can assess the importance of diffraction using a non-dimensional parameter, δ, first proposed by *Battjes* [1968]. Physically, this parameter represents an estimate of the normalized error in the wave phase speed when diffraction is neglected, and diffractive
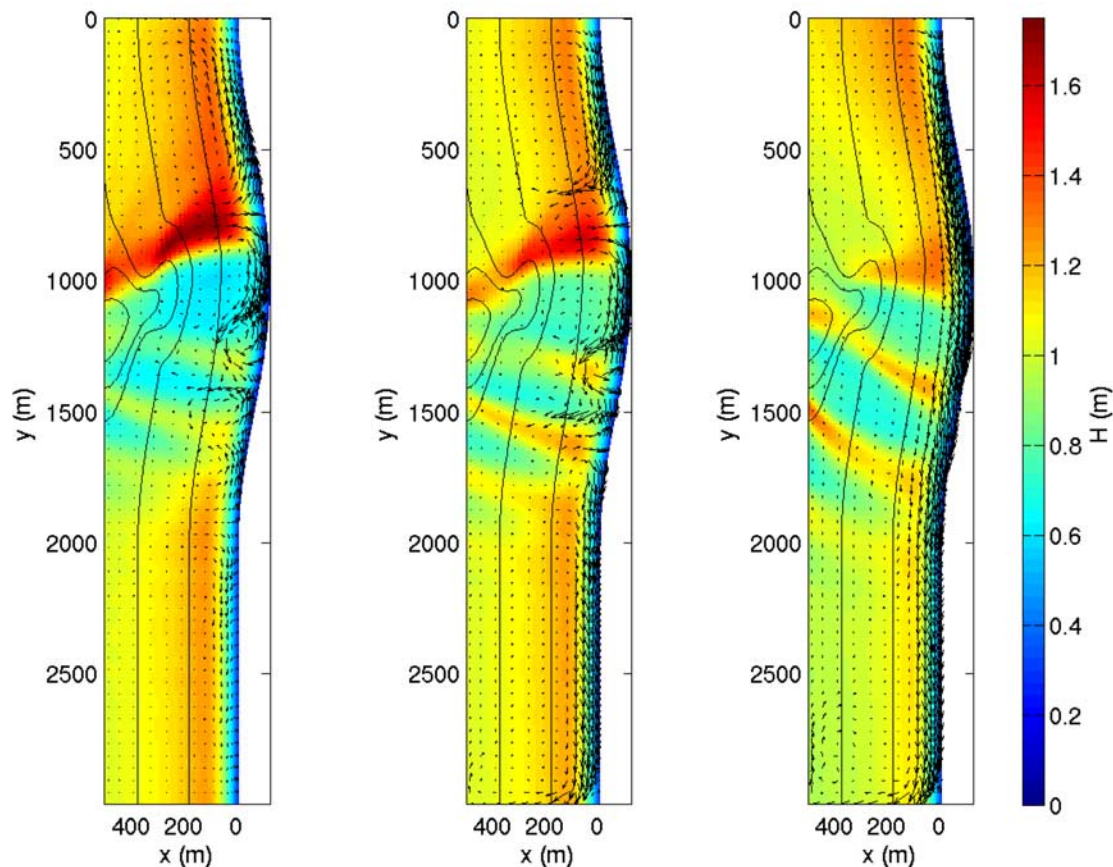
Figure 17. Predicted velocity field (black vectors) superimposed on the predicted root-mean-square wave height for the following wave conditions: JONSWAP spectrum with Hs = 1.5 m, T_p = 10s, γ = 10, m = 40 and (left) θ_p = 270 degrees (normally incident), (middle) θ_p = 285 degrees, (right) θ_p = 315 degrees. Depth contours (black) correspond to the 0, 5, 10, 15, 25, and 50 m contours.

effects are considered to be minor if $\delta \ll 1$. For the undulating canyon bathymetry, δ is generally less than 0.15 and reaches 0.2 in a few localized areas. We have further carried out limited simulations of the wave field on the idealized undulating bathymetry using the spectral refraction/diffraction model REF/DIF S and find that the wave height variations with O(100 m) length scales generated by the canyon undulations are still apparent when including diffractive effects. Also unaccounted for in this study is the effect of wave-current interaction. Recent studies have shown that considering wave-current interaction reduces the offshore extent of rip currents and may induce additional unsteadiness [*Haas et al.*, 2003; *Yu and Slinn*, 2003]. However, there is no evidence that wave-current interaction affects the alongshore position of rip currents. For our idealized cases we find that the circulation dynamics are linked to individual characteristics of the site, including shoreline curvature, canyon configuration and undulations in the canyon contours. The resulting circulation may be affected by changes to the curvature of the shoreline, amplitude of the contour undulations, or the location of the canyon relative to the shoreline. For instance, preliminary results show that canyon undulations of one-half the amplitude presented herein result in similar, though weaker, circulation patterns, while reducing the amplitude to one-quarter decreases the magnitude of the wave height

variations in the surf zone and significantly changes the predicted circulation patterns. The sensitivity of the nearshore circulation to these factors will remain a topic for future research and could result in guidelines regarding the attention that should be paid to such offshore features at a given site. Also of interest is the effect of the friction coefficient in the development of predicted circulation patterns. For the simulations shown herein, the friction coefficient (c_f = 0.003) was chosen such that reasonable current magnitudes (O(1 m/s)) were obtained. However, we also performed a preliminary simulation where the friction coefficient was increased by a factor of 2 and found that the strength of the circulation field was reduced by an order of magnitude. Further, the rip current locations correspond more closely to those obtained using the linear circulation model, which is expected because weak current velocities are associated with small nonlinearity. Our results reiterate the relationship between bottom friction and inertial effects and the role they have in dictating rip current locations. They also highlight the need for future research in studying frictional effects in the field.

6. Conclusions

[28] In this study, we were motivated by simulations of the wave and circulation field during the Nearshore Canyon
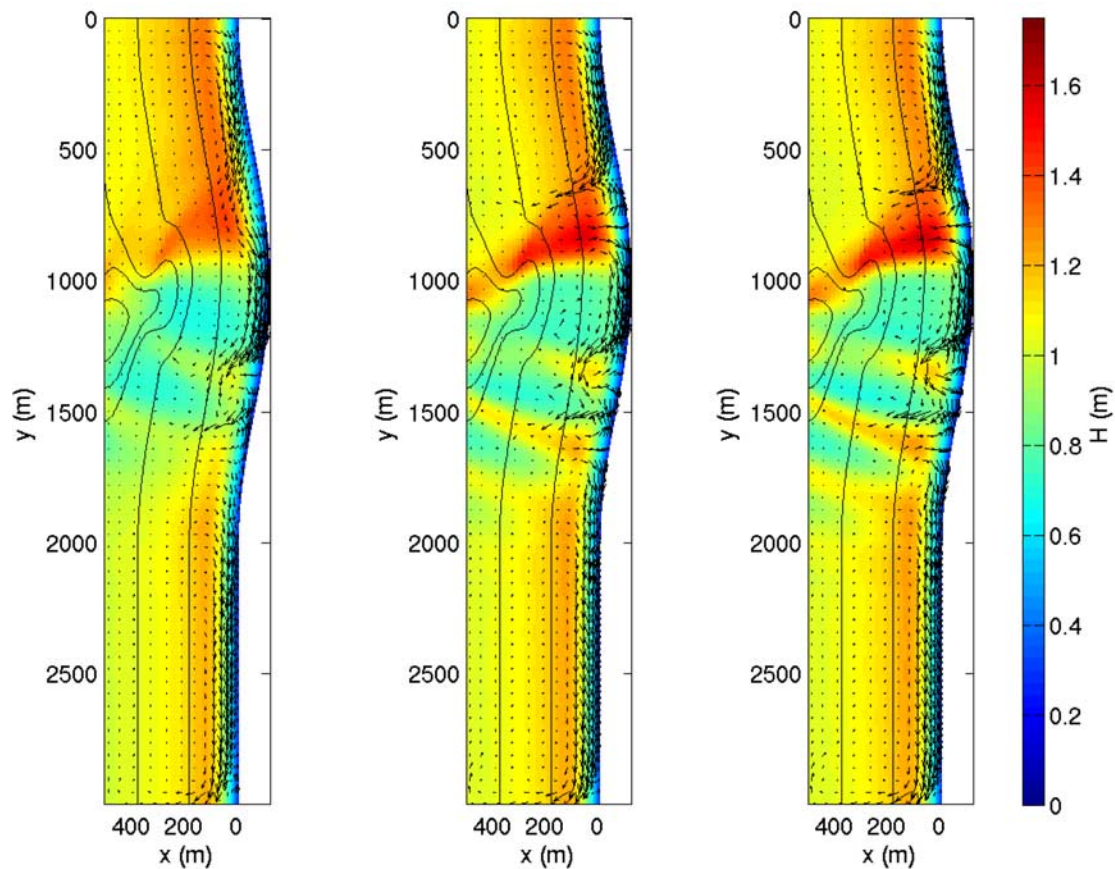
Figure 18. Predicted velocity field (black vectors) superimposed on the predicted root-mean-square wave height for the following wave conditions: JONSWAP spectrum with $Hs = 1.5$ m, $T_p = 10$s, $\theta_p = 285$ degrees, $\gamma = 10$, and (left) $m = 4$, (middle) $m = 24$, (right) $m = 40$. Depth contours (black) correspond to the 0, 5, 10, 15, 25, and 50 m contours.

Experiment which indicated that features of the circulation field could be closely tied to undulations in the offshore canyon and that the predicted rip currents showed correspondence with rip currents observed in the NCEX video data. We further performed a sequence of idealized tests to determine the relative importance of the large-scale structure of offshore bathymetric features (i.e. submarine canyons) and the finer details of those features (i.e. undulations) in controlling rip current location. These case studies showed that it was the specific details of the offshore bathymetry that dictated the refraction patterns responsible for driving rip currents in particular locations and that the number of rip currents was drastically reduced when no undulations were present. In other words, the development of the rip currents was controlled by the contour undulations rather than the presence of the submarine canyon. This suggests that rip currents could also be present for situations with undulating offshore contours that are, on average, parallel to the shoreline of an otherwise planar bathymetry. This result was, in fact, obtained in early simulations for such a simplified bathymetry. This finding has important ramifications for nearshore scientists because often times highly resolved surveys are only conducted in the surf zone where in-situ data is concentrated. In situations where the offshore

bathymetry dictates nearshore circulation patterns, future modeling efforts will be hindered without high-resolution offshore surveys. Our analyses for various offshore wave conditions indicate that the presence of rip currents is closely tied to the period and direction of the incident waves. In particular, we found that waves with relatively short periods are generally unaffected by the presence of the canyon and rip currents do not form. Similarly, waves approaching at large angles of incidence induce a strong alongshore current which dominates the nearshore circulation. Evaluation of the alongshore momentum balances indicates that the traditional balance outside the surf zone between the incident wave forcing and gradient in the mean water level is preserved, except where the rip current jet exits the surf zone and nonlinearity is dominant. Similarly, inside the surf zone and away from the circulation cell the balance is between the incident wave forcing and competing bottom friction. Within the circulation cell, either inside or outside of the surf zone, we see that the advective acceleration terms balance a large portion of the alongshore pressure gradient with bottom friction accounting for the remainder, indicating that the inertia of the current is important. The alongshore momentum balances also show that the initial rip current location is dictated by a balance between the gradients in
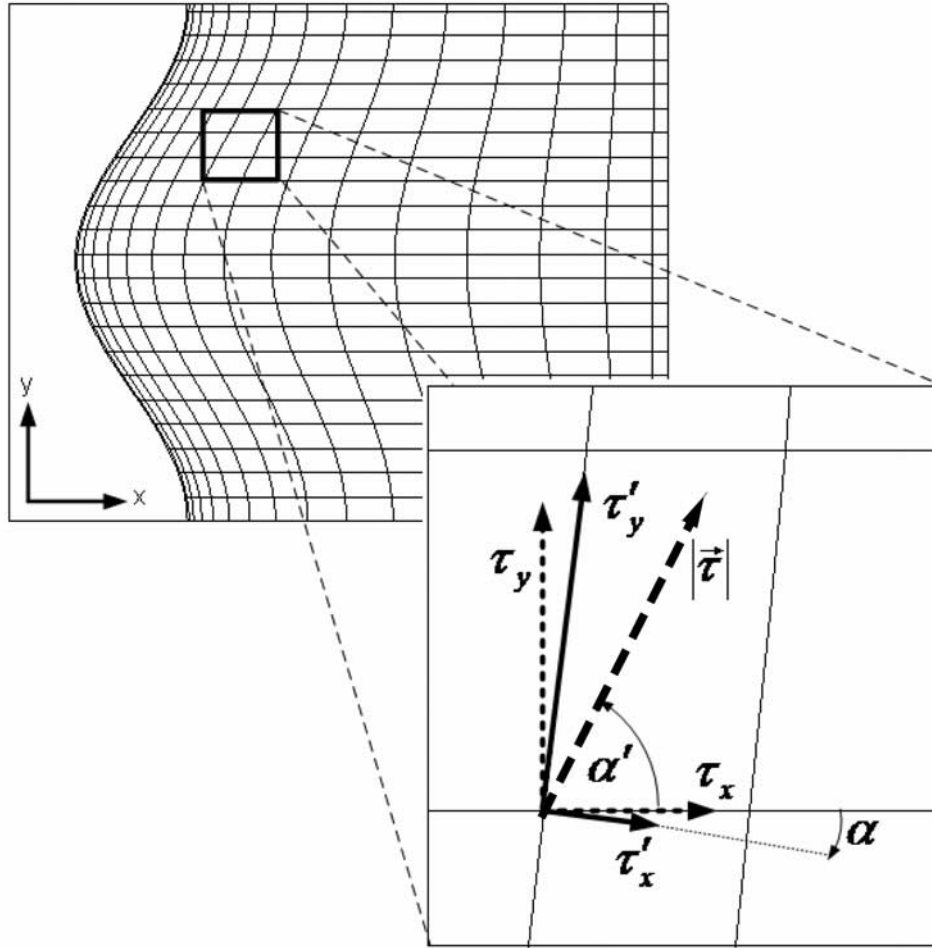
Figure B1. Transformation of model output vectors to a locally orthogonal system. τ_y and τ_x are the model output, $|\tau|$ is the resultant vector, and τ'_y and τ'_x are the translated orthogonal components of the resultant vector. The angle α' is measured between the model x-coordinate of the computational grid and the resultant vector and α is measured between the x-coordinate of the computational grid and the locally orthogonal x-coordinate.

radiation stress forcing and the pressure gradient induced by variations in the mean water surface elevation. Nonlinear processes, however, arise within minutes of the start of the simulation and have a pronounced effect on dictating the final location of the rip current. Hence, inertial effects are important in determining rip current location, and a nonlinear modeling scheme is generally required for accurate predictions of rip current location.

Appendix A: Bathymetric Equations

[29] The theoretical bathymetries were constructed using the following superposition of a planar beach, oblique elliptical canyon, and curved shoreline. In the following, x' points onshore and y' forms a right-handed coordinate system:

$$h = (h_o - mx') + f_c(x',y') + f_s(x',y') \qquad (A1)$$

where:

h_o = offshore water depth of the planar beach (97 m for all cases)

x'_c = slope of the planar beach (0.025 m/m for all cases)

$f_c(x', y')$ = function describing the elliptical canyon

$$= h_c \cdot \exp\left\{ -\frac{(x' - x'_c)^{20}}{L_{x'c}^{20}} \right\} \cdot \exp\left\{ -\frac{(y' - y'_c)^2}{L_{y'c}^2} \right\} \qquad (A2)$$

where:

h_c = maximum canyon depth (at center) (125 m for all cases)

x'_c = x-coordinate of the center of the canyon

$L_{x'c}$ = width of the canyon in cross-shore direction

y'_c = y-location of the canyon's major axis

$L_{y'c}$ = width of the canyon in cross-shore direction

$f_s(x', y')$ = function describing the curved shoreline

$$= h_s(y') \cdot \exp\left\{ -\frac{9}{2}\left(\frac{x' - 4000}{4000}\right)^2 \right\} \qquad (A3)$$

where:

$$h_s(y') = \begin{cases} -1.5 & y' < 1495 \text{ m} \\ -1.5\cos\left(\frac{2\pi(y' - 1495)}{2000}\right) & 1495 \text{ m} \le y' \le 3495 \text{ m} \\ -1.5 & y' > 3500 \text{ m} \end{cases}$$

A1. Curved Shoreline

[30] For the case with only a curved shoreline, the canyon depth is equal to zero and the equation collapses to:

$$h = (h_o - mx') + f_s(x', y') \qquad (A4)$$

A2. Curved Shoreline and Smooth Oblique Canyon

[31] The full expression in (A1) is used for this case with the parameters of the canyon as follows:

$$
\begin{aligned}
x'_c &= -650 \text{ m} \\
L_{x'c} &= 4000 \text{ m} \\
y'_c &= \tfrac{5}{8}(x' + 390) \text{ m} \\
L_{y'c} &= 125 \text{ m}
\end{aligned}
$$

A3. Curved Shoreline and Undulating Oblique Canyon

[32] The full expression (A1) is used for this case with the parameters of the canyon as follows:

$$
\begin{aligned}
x'_c &= -650 \text{ m} \\
L_{x'c} &= 4000 \text{ m} \\
y'_c &= \tfrac{5}{8}(x' + 390) \text{ m} \\
L_{y'c} &= 125 \cdot w(x') \cdot \sin(\tfrac{x'}{40}) \text{ m}
\end{aligned}
$$

where:

$$
w(x') = \begin{cases}
\dfrac{65}{2}\left(1 - \cos\left(\dfrac{2\pi(x' + dx')}{6000}\right)\right) & 0 \le x' \le 3000 \text{ m} \\
65 & x' > 3000 \text{ m}
\end{cases}
$$

Appendix B: Orthogonal Conversions

[33] We establish a domain bounded by a curved shoreline where the curvature of the gridlines is then damped exponentially with offshore distance. Orthogonality on this physical grid is accomplished using the local gradient of the gridlines at each node and the x and y components of each computed term in the momentum equation given below in vector form (B1):

$$\left\langle \frac{\partial \vec{u}}{\partial t} \right\rangle + \langle (\vec{u} \cdot \nabla)\vec{u} \rangle = \langle -g\nabla\eta \rangle + \langle \vec{\tilde{\tau}} \rangle + \langle \vec{\tau'} \rangle + \langle \vec{\tau_b} \rangle \quad (B1)$$

where the $\langle\ \rangle$ indicates a time-averaged quantity, η represents the mean water surface elevation, $\tilde{\tau}$ the incident wave forcing derived by *Longuet-Higgins and Stewart* [1964], τ' the lateral mixing term, and τ_b represents the bottom friction component. With knowledge of the appropriate angles, the output vectors can be translated to the desired orthogonal components. A schematic of the output vectors and the translated components is given in Figure B1. The corresponding equations are provided in (B2).

$$\tau'_x = |\vec{\tau}|\cos(\alpha - \alpha') \quad \tau'_y = |\vec{\tau}|\sin(\alpha - \alpha') \qquad (B2)$$

where τ'_x and τ'_y are the translated orthogonal vectors at each grid point, $|\vec{\tau}| = \sqrt{\tau_x^2 + \tau_y^2}$ is the magnitude of the original model output of each individual momentum term, α' is the angle measured between $|\vec{\tau}|$ and the x-axis of

the computational grid, and α is the angle between the x-coordinate of the computational grid and x-coordinate of the locally orthogonal grid.

References

Battjes, J. (1968), Refraction of water waves, *J. Waterw. Harbors Div. Am. Soc. Civ. Eng.*, WW4, 437–451.

Battjes, J. (1975), Modeling of turbulence in the surf zone, in *Proceeedings of Symposium on Modeling Techniques: Second Annual Symposium of the Waterways, Harbors, and Coastal Engineering Division of ASCE*, vol. 2, pp. 1050–1061, Am. Soc. of Civ. Eng., New York.

Booij, N., R. C. Ris, and L. H. Holthuijsen (1999), A third-generation wave model for coastal regions: 1. Model description and validation, *J. Geophys. Res.*, 104(C4), 7649–7666.

Bowen, A. J. (1969), Rip currents, *J. Geophys. Res.*, 74(23), 5467–5477.

Bowen, A. J., and D. L. Inman (1969), Rip currents: 2. Laboratory and field observations, *J. Geophys. Res.*, 74, 5479–5490.

Chickadel, C. C., R. A. Holman, and M. H. Freilich (2003), An optical technique for the measurement of longshore currents, *J. Geophys. Res.*, 108(C11), 3364, doi:10.1029/2003JC001774.

Dail, H. J., M. A. Merrifield, and M. Bevis (2000), Steep beach morphology changes due to energetic wave forcing, *Mar. Geol.*, 162, 443–458.

Dalrymple, R. A. (1975), A mechanism for rip current generation on an open coast, *J. Geophys. Res.*, 80, 3485–3487.

Haas, K. A., I. A. Svendsen, M. C. Haller, and Q. Zhao (2003), Quasi-three-dimensional modeling of rip current systems, *J. Geophys. Res.*, 108(C7), 3217, doi:10.1029/2002JC001355.

Haller, M. C., R. A. Dalrymple, and I. A. Svendsen (2002), Experimental study of nearshore dynamics on a barred beach with rip channels, *J. Geophys. Res.*, 107(C6), 3061, doi:10.1029/2001JC000955.

Hasselman, K., et al. (1973), Measurements of wind-wave growth and swell decay during the Joint North Sea Wave Project (JONSWAP), *Dtsch. Hydrogr. Z. Suppl.*, 12, A8.

Hino, M. (1974), Theory on the formation of rip current and cuspidal coast, in *Proceedings of 14th Coastal Engineering Conference*, pp. 901–919, Am. Soc. of Civ. Eng., New York.

Holman, R. A., A. H. Sallenger Jr., T. C. Lippmann, and J. W. Haines (1993), The application of video image processing to the study of nearshore processes, *Oceanography*, 6, 78–85.

Lippmann, T. C., and R. A. Holman (1989), Quantification of sand bar morphology: A video technique based on wave dissipation, *J. Geophys. Res.*, 94(C1), 995–1011.

Longuet-Higgins, M. S., and R. W. Stewart (1964), Radiations stresses in water waves; a physical discussion, with applications, *Deep Sea Res.*, 2, 529–562.

Morton, R. A., M. P. Leach, J. G. Paine, and M. A. Cardoza (1993), Monitoring beach changes using GPS surveying techniques, *J. Coastal Res.*, 9, 702–720.

Özkan-Haller, H. T., and J. T. Kirby (1997), A Fourier-Chebyshev collocation method for the shallow water equations including shoreline runup, *Appl. Oceanic Res.*, 19, 21–34.

Özkan-Haller, H. T., and J. T. Kirby (1999), Nonlinear evolution of shear instabilities of the longshore current: A comparison of observations and computations, *J. Geophys. Res.*, 104, 25,953–25,984.

Plant, N. G., K. T. Holland, and J. A. Puleo (2002), Analysis of the scale of errors in nearshore bathymetry data, *Mar. Geol.*, 191, 71–86.

Seymour, R. J., M. H. Sessions, and D. Castel (1985), Automated remote recording and analysis of coastal data, *J. Waterw. Port Coastal Ocean Eng.*, *111*(2), 388–400.

Shepard, F. P., and D. L. Inman (1950), Nearshore circulation, *Coastal Eng.*, 50–59.

Shepard, F. P., K. O. Emery, and E. C. LaFond (1941), Rip currents: A process of geological importance, *J. Geol.*, *49*, 337–369.

Smith, G., D. Darnell, J. Magalen, J. Long, and T. Lippmann (2003), Shallow water bathymetry measured during NCEX, *Eos Trans. AGU*, *84*(46), Ocean Sci. Meet. Suppl., Abstract OS32F-04.

Yu, J., and D. N. Slinn (2003), Effects of wave-current interaction on rip currents, *J. Geophys. Res.*, *108*(C3), 3088, doi:10.1029/2001JC001105.

_____

J. W. Long and H. T. Özkan-Haller, College of Oceanic and Atmospheric Sciences, Oregon State University, 104 Ocean Admin. Building, Corvallis, OR 97331-5503, USA. (jlong@coas.oregonstate.edu)